Tran-SET

Transportation Consortium of South-Central States

Solving Emerging Transportation Resiliency, Sustainability, and Economic Challenges through the Use of Innovative Materials and Construction Methods: From Research to Implementation

Sustainability-Based Long-Term Management of Bridges under Multi-Hazard Exposure

Project No. 17STOKS01

Lead University: Oklahoma State University

Preserving Existing Transportation Systems

Final Report

November 2018

Disclaimer

The contents of this report reflect the views of the authors, who are responsible for the facts and the accuracy of the information presented herein. This document is disseminated in the interest of information exchange. The report is funded, partially or entirely, by a grant from the U.S. Department of Transportation's University Transportation Centers Program. However, the U.S. Government assumes no liability for the contents or use thereof.

Acknowledgments

The support and directions of the Project Review Committee Members Dr. Samer El-Bahey, Dr. Aman Karamlou, and Dr. Georgios Tsampras are greatly acknowledged. The authors wish to thank Dr. Esther Mullens of the South Central Climate Science Center, University of Oklahoma, for the valuable information provided in support of this study.

TECHNICAL DOCUMENTATION PAGE

1. **Project No.**	**2. Government Accession No.**	**3. Recipient's Catalog No.**
17STOKS01		

4. Title and Subtitle	**5. Report Date**
Sustainability-Based Long-Term Management of Bridges under Multi-Hazard Exposure	Nov. 2018
	6. Performing Organization Code
7. Author(s)	**8. Performing Organization Report No.**
PI: Mohamed Soliman https://orcid.org/0000-0003-3160-0933 GRA: Omid Khandel https://orcid.org/0000-0003-2204-340X	
9. Performing Organization Name and Address	**10. Work Unit No. (TRAIS)**
Transportation Consortium of South-Central States (Tran-SET) University Transportation Center for Region 6 3319 Patrick F. Taylor Hall, Louisiana State University, Baton Rouge, LA 70803	**11. Contract or Grant No.** 69A3551747106
12. Sponsoring Agency Name and Address	**13. Type of Report and Period Covered**
United States of America Department of Transportation Research and Innovative Technology Administration	Final Research Report May 2017 – May 2018
	14. Sponsoring Agency Code

15. Supplementary Notes

Report uploaded and accessible at: Tran-SET's website (http://transet.lsu.edu/)

16. Abstract

Bridges are under deterioration due to various mechanical and environmental stressors. Hydraulic-related hazards (e.g., flood and scour), aggressive environmental conditions, and seismic events (e.g., earthquake) are recognized as the most significant threats to the safety of bridges. In traditional risk assessment methods for structures susceptible to damage due to floods and other natural hazards (e.g., corrosion and seismic events), future hazard predictions are conducted using historic return periods and climate records. However, recent increase in flood intensity in central-southern states indicate that future hazard occurrence rate may not necessarily follow past trends. Accordingly, current design, assessment, and management methodologies should adapt to these changes in order to ensure the satisfactory performance of bridges under the combined or cumulative action of hazards. This project addresses this need by presenting a framework for risk quantification and optimum management of bridges susceptible to damage due to floods, flood induced scour, and other gradual deterioration mechanism (e.g., corrosion and fatigue). Downscaled climate data, adopted from the global climate models, are employed to predict future flood hazard at a given location. Probabilistic simulation is used to quantify the time-dependent failure probability, which subsequently helps quantify the long-term sustainability through the systematic integration of economic, social, and environmental metrics associated with bridge failures. These profiles can be next used to obtain optimum interventions required to extend the service life while maintaining the structural performance above prescribed thresholds.

17. Key Words	**18. Distribution Statement**
Multi-Hazard, Risk, Climate Change, Corrosion, Scour	No restrictions.

19. Security Classif. (of this report)	**20. Security Classif. (of this page)**	**21. No. of Pages**	**22. Price**
Unclassified	Unclassified	44	

Form DOT F 1700.7 (8-72) **Reproduction of completed page authorized.**

SI* (MODERN METRIC) CONVERSION FACTORS

APPROXIMATE CONVERSIONS TO SI UNITS

Symbol	When You Know	Multiply By	To Find	Symbol
		LENGTH		
in	inches	25.4	millimeters	mm
ft	feet	0.305	meters	m
yd	yards	0.914	meters	m
mi	miles	1.61	kilometers	km
		AREA		
in^2	square inches	645.2	square millimeters	mm^2
ft^2	square feet	0.093	square meters	m^2
yd^2	square yard	0.836	square meters	m^2
ac	acres	0.405	hectares	ha
mi^2	square miles	2.59	square kilometers	km^2
		VOLUME		
fl oz	fluid ounces	29.57	milliliters	mL
gal	gallons	3.785	liters	L
ft^3	cubic feet	0.028	cubic meters	m^3
yd^3	cubic yards	0.765	cubic meters	m^3
		NOTE: volumes greater than 1000 L shall be shown in m^3		
		MASS		
oz	ounces	28.35	grams	g
lb	pounds	0.454	kilograms	kg
T	short tons (2000 lb)	0.907	megagrams (or "metric ton")	Mg (or "t")
		TEMPERATURE (exact degrees)		
^oF	Fahrenheit	5 (F-32)/9 or (F-32)/1.8	Celsius	^oC
		ILLUMINATION		
fc	foot-candles	10.76	lux	lx
fl	foot-Lamberts	3.426	candela/m^2	cd/m^2
		FORCE and PRESSURE or STRESS		
lbf	poundforce	4.45	newtons	N
lbf/in^2	poundforce per square inch	6.89	kilopascals	kPa

APPROXIMATE CONVERSIONS FROM SI UNITS

Symbol	When You Know	Multiply By	To Find	Symbol
		LENGTH		
mm	millimeters	0.039	inches	in
m	meters	3.28	feet	ft
m	meters	1.09	yards	yd
km	kilometers	0.621	miles	mi
		AREA		
mm^2	square millimeters	0.0016	square inches	in^2
m^2	square meters	10.764	square feet	ft^2
m^2	square meters	1.195	square yards	yd^2
ha	hectares	2.47	acres	ac
km^2	square kilometers	0.386	square miles	mi^2
		VOLUME		
mL	milliliters	0.034	fluid ounces	fl oz
L	liters	0.264	gallons	gal
m^3	cubic meters	35.314	cubic feet	ft^3
m^3	cubic meters	1.307	cubic yards	yd^3
		MASS		
g	grams	0.035	ounces	oz
kg	kilograms	2.202	pounds	lb
Mg (or "t")	megagrams (or "metric ton")	1.103	short tons (2000 lb)	T
		TEMPERATURE (exact degrees)		
^oC	Celsius	1.8C+32	Fahrenheit	^oF
		ILLUMINATION		
lx	lux	0.0929	foot-candles	fc
cd/m^2	candela/m^2	0.2919	foot-Lamberts	fl
		FORCE and PRESSURE or STRESS		
N	newtons	0.225	poundforce	lbf
kPa	kilopascals	0.145	poundforce per square inch	lbf/in^2

TABLE OF CONTENTS

LIST OF FIGURES

ACRONYMS, ABBREVIATIONS, AND SYMBOLS

AASHTO	American Association of State Highway and Transportation Officials
BCCA	Daily Bias Correction Constructed Analogs
BSCD	Bias and Spatial Downscaling Correction
CA	Constructed Analogues
CMIP5	Coupled Model Inter-Comparison Project Phase 5
DIN	Dissolved Inorganic Nitrogen
FHWA	Federal Highway Administration
GHG	Greenhouse Gas
MCS	Monte Carlo Simulation
NOAA	National Oceanic and Atmospheric Administration
NSHMP	National Seismic Hazard Model Project
PDF	Probability Distribution Function
RCP	Representative Concentration Pathways
USGS	United States Geological Survey
VIC	Variable Infiltration Capacity

U_k	Effective Rainfall
c	Mass Balance
ϕ_k	Soil Moisture Index
l	Soil Moisture Index Threshold
p	Nonlinear Response Term
r_k	Observed Rainfall
τ_k	Drying Rate
τ_w	Reference Drying Rate
f	Temperature Modulation
T_r	Reference Temperature
T_k	Drying Temperature
Q_k	Streamflow

α	Storage Coefficient
β	Fraction of Effective Rainfall
δ	Delay between the Rainfall and Streamflow
z	Time-step Shifter
a_i	Fitted Parameter
b_i	Fitted Parameter
R^2	R Squared
Q_o	Observed Streamflow Value
Q_M	Modeled Streamflow Value
V_{appr}	Water Velocity at the Location of Interest
D	Pier Diameter
Z_{max}	Maximum Pier Scour
V_{max}	Maximum Water Velocity
v	Kinematic Viscosity of Water
Re	Reynolds Number
H_L	Ultimate Lateral Load Carrying Capacity of One Pile
η	Shape Factor
K_p	Passive Earth Pressure Coefficient
K	Lateral Earth Pressure Coefficient
δ	Interface Friction Angle between the Pile and Soil
γ	Effective Unit Weight of Soil
a	Depth to the Point of Rotation
B	Diameter or Width of the Pile
L	Embedded Length of Pile
e	Eccentricity of Loading
R_s	Shaft Resistance
R_p	Toe Resistance
f_s	Unit Shaft Resistance
A_s	Pile Shaft Surface Area

q_p	Unit Toe Resistance
A_p	Pile Toe Area
F_L	Flood-Induced Lateral Load
A	Area of Accumulated Debris
P	Water Pressure on Piers
C_D	Drag Coefficient
V_{appr}	Velocity of Stream Flow
$G_L(t)$	Lateral Performance Functions at time t
$G_V(t)$	Vertical Performance Functions at time t
$H_L(t)$	Respective Time-Variant Lateral Capacity
$R_V(t)$	Time-Variant Vertical Capacity
$F_L(t)$	Lateral Load Effects at Time t
$F_V(t)$	Vertical Load Effects at Time t
$P_f(t)$	Point in Time Probability of Failure
$g_i(t)$	ith Performance Function
$TDP(y)$	Cumulative Annual Probability of Failure
$Risk\ (t)$	Time Dependent Risk
C	Monetary Value Associated with Bridge Failure
C_{reb}	Rebuilding Cost
C_{run},	Running Cost
C_{tl}	Time Loss
C_{rc}	Rebuilding Cost per Unit Area
W_b	Bridge Width
L_b	Bridge Length
C_{rv}	Average Cost of Running Vehicle
D	Detour Length
ADT	Average Daily Traffic
D	Duration of Detour
C_1	Value of Time per Adult

C_2	Value of Time for Truck
S	Average Detour Speed
T	Average Daily Truck Traffic (%)
O	Occupancy Rate
C_s	Y-Intercept at Time Zero of the Long Term Corrosion Rate
R_s	Slope of the Long Term Corrosion Rate
$C(t)$	Time Dependent Corrosion Loss
t_{sl}	Service Life
t_{maint}	Time of Maintenance Action

EXECUTIVE SUMMARY

Natural hazards (e.g., floods, scours, and earthquakes), environmental stressors (e.g., corrosive environments), or human-induced extreme events (e.g., fire and blasts) are the main sources that drive bridge deterioration or failure. A full or partial bridge failure may disrupt the transportation network connectivity leading to significant economic, social, or environmental impacts. Accordingly, maintenance and retrofit planning is required to minimize the risk of bridge failure and maximize the safety of transportation networks. However, this planning process is influenced by several sources of uncertainty that can affect the decision-making process. Quantifying and minimizing uncertainties associated with hazard prediction and deterioration modeling is essential for proper maintenance planning.

Risk-based infrastructure management approaches provide the necessary mechanisms to evaluate the combined or cumulative effects of different hazards on the structural performance. These probabilistic approaches provide a systematic mechanism for considering different sources of uncertainties associated with bridge maintenance and management activities. An essential task in these procedures is to develop a reasonable prediction of the future occurrence rate associated with different hazards. In this context, climate change is expected to affect the long-term precipitation trends and alter the occurrence probability of riverine flooding. Other deterioration mechanisms, such as corrosion propagation, can also be affected by climate change. With the change in the deterioration patterns caused by climate change, the bridge ability to resist loading effects of other hazards (e.g., seismic events) may be reduced. Accordingly, it is essential to develop a methodology that can predict structural performance and failure risk under the combined effect of multiple hazards.

This report presents a probabilistic framework for quantifying the risk of bridge failure under sudden or gradual deterioration mechanisms such as floods, flood-induced scours, and marine or freshwater corrosion. The effect of long-term climate changes on flood hazards and corrosion propagation are considered. Global Climate Models (GCMs) are used to predict future precipitation and temperature profiles. Downscaled precipitation and temperature climate data for the location of interest during the time span of 1960 to 2100 are adopted from Coupled Model Inter-comparison Project Phase 5 (CMIP5) archive. A hybrid conceptual-metric tool is used to establish streamflow profiles based on the adopted climate datasets. Corrosion propagation rate and scour depth profiles are developed using the predicted temperature and streamflow profiles. The time-dependent corrosion propagation and scour predictions are then used to quantify the axial and lateral capacities of the bridge foundations. Point-in-time and cumulative probabilities of failure are estimated based on the lateral and axial performance functions in terms of resistance and load effects. Consequences of bridge failure considering direct (i.e., structural rehabilitation costs) and indirect sustainability metrics are employed to establish the time-dependent risk profiles. The proposed bridge failure risk quantification approach presented in this study is applied to an existing bridge in Oklahoma.

Additionally, an integrated framework for establishing the optimum maintenance strategies considering climate change effects is introduced and discussed in this report. This framework is capable of minimizing the total life-cycle cost and providing an optimal maintenance plan for bridges under combined effects of different deterioration mechanisms.

IMPLEMENTATION STATEMENT

The implementation and workforce development activities related to this project were conducted on three fronts: (a) active dissemination of the research methodology and results, (b) translating the developed approaches into classroom material, and (c) developing a step-by-step procedure to apply the developed methodology. These activities ensure the smooth transition of the proposed approach from the research to implementation.

As part of the activities to disseminate the developed approach, the following presentations and papers were published/presented as part of the project funded by Tran-SET:

- Khandel, O. & Soliman, M., (2019). An Integrated Framework for Quantifying the Effect of Climate Change on the Risk of Bridge Failure due to Floods and Flood-induced Scour, (under review).
- Khandel, O. & Soliman, M., (2019). Multi-hazard Risk Assessment of Bridges Considering Climate Change, *Proceedings of the 2019 Tran-SET Conference*, San Antonio, TX, April 11-12, 2019 (submitted).
- Ali, H. & Soliman, M. (2018). Reliability Analysis of Steel Bridges under Propagating Fatigue Cracks, *Proceedings of the 98th International Conference on Bridge Maintenance, Safety and Management (IABMAS 2018).* Melbourne, Australia, July 9-13, 2018 (accepted).
- Khandel, O. & Soliman, M., (2018). Maintenance Optimization for Deteriorating Bridges under Uncertainty, *Proceeding of ASCE-SEI 2018 – Structures Congress 2018*. Fort Worth, Texas, USA, April 16-19, 2018.
- Khandel, O. & Soliman, M., (2018). Multi-hazard Risk Analysis of Bridges Considering Climate Change, *Proceeding of 2018 Tran-SET Conference*. New Orleans, Louisiana, USA, April 3-4, 2018.
- Khandel, O. & Soliman, M., (2017). *Effect of Climate Change on the Risk of Bridge Failure due to Flood and Flood-induced Scour*, Poster presented at the OTRD 2017 - Oklahoma Transportation Research Day, Oklahoma City, OK, USA, October 17, 2017.

As part of the educational activities related to this project, the PI added a module to the "Reliability and Risk of Components and Systems" class, offered during the Fall of 2017 (annually thereafter), related to sustainability-based risk management under extreme events, which is heavily based on the research developed in this project.

Finally, a step-by-step guide is currently under preparation and will be presented to the Oklahoma Department of Transportation (ODOT) during the implementation period of this project.

1. INTRODUCTION

Bridges are under deterioration due to various mechanical and environmental stressors. Hydraulic-related hazards (e.g., floods and scours), aggressive environmental conditions, and seismic events (i.e., earthquakes) are recognized as the most significant threats to the safety of bridges. In traditional risk assessment methods for structures susceptible to damage due to floods and other natural hazards (e.g., corrosion and seismic events), future hazard predictions are conducted using historic return periods and climate records. However, the recent increase in flood intensity in central-southern states indicates that the future hazard occurrence rate may not necessarily follow past trends. Accordingly, current design, assessment, and management methodologies should adapt to these changes in order to ensure the satisfactory performance of bridges under the combined or cumulative action of hazards. This project addresses this need by presenting a framework for optimum management of bridges susceptible to damage due to floods, and other gradual deterioration mechanisms (e.g., corrosion and fatigue). Downscaled climate data, adopted from the global climate models, are employed to predict future flood hazard at a given location. Probabilistic simulation is used to quantify the time-dependent failure probability, which subsequently helps quantifying the long-term sustainability through the systematic integration of economic, social, and environmental metrics associated with bridge failures or interventions. These profiles can be next used to obtain optimum times and types of interventions required to extend the service life while maintaining the structural performance above prescribed thresholds.

The increase in flood frequency and intensity, which may be attributed to the climate change, is adversely affecting the safety of our Nation's bridges and imposing devastating consequences to our transportation systems and the communities which they serve. As an indication of the severity of this problem, the 2015 flooding in Texas and Oklahoma led to at least five reported complete or partial bridge failures *(1)*. In 2017, Hurricane Harvey caused severe flooding which led to the failure of several bridges in Texas. This 2017 flooding in Houston, Texas was considered the third 500-year flood to occur within the preceding three years. These events highlight the extent of increase in the occurrence rate of high intensity weather-related extreme events. In order to prevent failure of bridges due to these extreme events, bridge design and management approaches should account for the increase in the hazard occurrence rates in affected states. Retrofit and maintenance activities should be optimally planned to reduce the failure risk and minimize the impact of bridge interventions on the economic, social, and environmental systems.

2. OBJECTIVES

The main objective of the proposed research is to develop a sustainability-based framework for management of bridges under multi-hazard exposure. In more detail, the proposed research aims to:

(a) Develop a comprehensive integrated tool to assess the risk of failure for bridges under multiple hazards. The tool is capable of integrating multiple hazards in a risk-based framework. Social, economic, and environmental sustainability measures are also included in the risk prediction.

(b) Introduce a precise, yet computationally efficient probabilistic framework for quantifying the risk of bridge failure under climate change. The proposed approach is suitable for assessing the long-term risk of bridge failure under flood loads, as well as other climate-related hazards.

(c) Provide an approach for optimal decision-making under uncertainty to establish optimum management activities of bridges considering sustainability metrics.

(d) Establish a detailed guideline for optimal sustainability-based management of deteriorating bridges.

3. SCOPE

The research work presented herein focuses on water-crossing steel and concrete bridges located in Region 6. In Oklahoma, Northern Texas, Arkansas, and Louisiana, intense precipitation is frequent and usually leads to riverine flooding and bridge failures. The reported research covers sudden hazards (e.g., floods) and gradual deterioration (e.g., corrosion). For flood hazard, considered failure mechanisms include hydrodynamic horizontal forces on superstructure, debris effect, failure of substructure due to accelerated flood-induced scour, and the coupled effects of these mechanisms. The effect of time-dependent scour deterioration is considered in evaluating cumulative time-dependent risk of failure the investigated bridge. Gradual deterioration due to aggressive environmental conditions such as corrosion is included. The approach is applied to a case study located on the Oklahoma-Texas border. The case study represents a steel girder bridge with deep foundations. However, the established approach is equally applicable to bridges with other structural systems at different locations.

4. METHODOLOGY

This report aims to provide a probabilistic framework for risk analysis of bridges susceptible to damage due to floods, flood-induced scours, and corrosive environment. The probability of failure under flood-induced loads is predicted considering climate change by utilizing downscaled data adopted from global climate models. The proposed framework can establish risk profiles which depict the time-dependent performance of the structure. Environmental, economic, and social sustainability metrics are integrated into the risk assessment by quantifying the monetary values associated with these metrics. The following subsections provide an in-depth discussion on the different modules of the framework.

4.1. Background

Bridges are under continuous deterioration due to various mechanical and environmental stressors. Among the various extreme events which may affect the safety of bridges, hydraulic-related ones have been identified as the leading cause of bridge failure *(2, 3)*. In the United States, statistical analysis estimates that 52% of bridge failures are attributed to hydraulic causes (e.g., flood and scour) *(4)*. Hydraulic bridge failures are related to precipitation patterns and flood events at the bridge location. In this context, the National Oceanic and Atmospheric Administration (NOAA) reports an average increase of 612% in the number of floods in the United States since the 1960s and it is expecting a future increase in this percentage *(5)*.

The increase in flood frequency and intensity, which may be attributed to the climate change, is expected to adversely affect the safety of our nation's bridges, along with devastating consequences to our transportation systems and the communities which they serve. As an indication of the severity of this problem, the 2015 flooding in Texas and Oklahoma led to at least five reported complete or partial bridge failures *(6, 7)*. These 2015 flood events resulted in 31 deaths and more than 2.5 billion dollars in economic losses to the region *(8)*. Accordingly, bridge design and management approaches should be constructed with the ability to account for climate change in the quantification of future flood hazard.

Flooding can damage the bridge in several ways including overtopping, accelerated scour, debris impact, erosion of bridge approaches, and failure due to horizontal direct water pressure. Among those, scour is the most difficult deterioration mode from the management viewpoint *(9)*. It can occur in any type of soil and undermines the stability of the bridge foundation. Accordingly, its effects are generally global, where the failure of one footing may lead to the progressive collapse of the whole structure. Moreover, it is very difficult to detect and manage since most of its effects are hidden under water. Scour exposes the bridge foundations and reduces the buckling resistance of piles, as well as the lateral capacity of the foundations. Additionally, bridges subjected to scour become more vulnerable during floods *(10)* and may also be vulnerable under other extreme events such as seismic excitations and traffic overload *(11, 12)*.

In addition to the impact that climate change may have on flood hazard occurrence probability, it can also affect the long-term corrosion propagation rate in structural components. For instance, *(13)* and *(14)* concluded that the long-term increase in temperatures affects the material diffusivity and consequently escalates the reinforcement corrosion rate in reinforced concrete (RC) structures. In addition, Chaves et al. *(15)* and Peng et al. *(16)* conducted

probabilistic analysis on corrosion of steel in marine structures considering global warming effects. The influence of seawater temperature and microbiological nutrients on corrosion propagation was investigated in these studies. The results of both studies highlight the impact of climate change on the long-term reliability of marine structures under corrosion deterioration.

Over the past decades, researchers have formulated methodologies to evaluate the scour at bridges either deterministically (e.g., *(17, 18)*) or probabilistically (e.g., *(19, 20)*), with detailed methodologies which can predict the performance of bridges deteriorated by scour under flood-induced loads. Other studies focused on evaluating the effect of scour on the response of bridges under other hazards such as seismic events or traffic overload (e.g., *(21-27)*). However, these studies did not focus on examining the potential influence of climate change on scour- or flood-vulnerable bridges. In an attempt to address this issue, Kallias and Imam *(28)* performed a parametric investigation to quantify the change in the failure probability of bridges with the change in the mean and standard deviation of the river flow. In another effort, Dong and Frangopol *(29)* presented an approach to quantify the risk of bridge failure and bridge resilience under multi-hazard exposure. Their study quantified the bridge risk under 100, 200, and 500 years flood hazard, however no future climate prediction was included.

Due to climate change, the uncertainties in the future projections of precipitation, temperature, regional moisture, rainfall, and river streamflow significantly increase, causing the traditional methods of design and assessment of bridges based on the 50, 100, or 200 year floods to be highly unreliable *(30)*. This unreliability promotes using a more dependable method for future climate prediction in order to assess the flood hazard and corrosion deterioration. Using the results of global climate modeling and downscaling techniques to derive the regional-scale data can help quantifying the flood hazard considering various climate-related parameters (e.g., carbon dioxide emission).

Global climate models (GCMs) are constructed using a general circulation model to simulate the atmosphere considering chemical, physical, and biological aspects of the global climate system *(31, 32)*. Several GCMs exist such as FIO-ESM, MPI_ESM_LR, CCSM4, MIROC5 and BNU-ESM *(33)*. The global climate modeling data are in global scale and they should be converted to regional scale data in order to study climate patterns associated with a given river basin. This can be achieved by running a higher resolution GCM, using boundary conditions of surrounding global climate model, or using statistical downscaling methods. The first two methods are generally recognized as more complicated and computationally expensive in comparison to statistical downscaling methods, which can still achieve results with sufficient accuracy *(34, 35)*. GCMs can also be constructed for different scenarios of future greenhouse gas (GHG) emission. Due to the presence of several GHG emission scenarios, different global climate modeling techniques, and downscaling methods, climate researchers recommend using several scenarios, each of which is characterized by its own future GHG emission level, global climate model, and downscaling technique to quantify the highest and lowest critical bounds for future climate trends *(36)*.

After obtaining the prediction of future climate trends and precipitation data, different hydrological models such as Variable Infiltration Capacity (VIC) *(37)*, RAPID *(38)*, and

Riverware *(39)* can be used to estimate the time-dependent river discharge and quantify the future flood hazard. This approach was implemented in *(40)* to quantify the impact of climate change on the Red River basin in Oklahoma. In *(40)*, three GCMS, GHG emission scenarios, and downscaling techniques have been implemented leading to 27 different climate scenarios. A similar approach has been implemented in a pilot study for Iowa Department of Transportation to quantify the increase in streamflow at different bridge locations within the state *(30)*. The report indicated that four of the six investigated bridges would be exposed to increased frequency of extreme streamflow and would have a higher frequency of overtopping.

However, the hydrologic modeling using these tools often requires significant effort in calibration and executing the analysis, significant experience in hydrologic modeling, and specialized software that may not be available to all engineers. Accordingly, applying such approaches to bridge risk assessment considerably increases the complexity of the analysis. Accordingly, an efficient, yet accurate approach is still needed for bridge risk assessment considering climate change, which is the main focus of this report.

4.2. Significance and Technical Contributions

This report presents a probabilistic framework for quantifying the effect of climate change on time-dependent risk of bridge failure under flood loads, flood-induced scours, and corrosion. The proposed approach utilizes the downscaled data adopted from Global Climate Models (GCMs) to obtain future temperature and discharge predictions under different climate scenarios. Future discharge is used to predict the scour depth and flood loads. The probability of failure under combined deterioration is computed using Monte Carlo Simulation (MCS) and the risk of bridge failure is quantified by combining the resulting probability of bridge failure and the consequences of bridge closure and/or failure. The proposed approach is applied to I-35 Red River bridge located on the Texas-Oklahoma border. The key technical contributions of the presented research can be listed as follows:

- Predicting future flood and flood-induced scour profiles by employing global climate models, and an efficient yet accurate streamflow prediction model
- Presenting a fully probabilistic framework for quantifying the effect of climate change on the bridge failure risk
- Predicting the long-term risk associated with the failure of the investigated bridge considering the exposure to multiple hazards (i.e., flood, flood-induced scour, and corrosive environment) and consequences of failure.

4.3. Climate Modeling

The greenhouse gas emission has seen a considerable increase through the 20^{th} century. The ozone layer depletion attributed to this increase causes noticeable change in climatic conditions including global temperature increase, sea level rise, and imbalance in precipitation patterns *(41, 42)*. Over the past decade, significant research has been conducted with the main goal of predicting future climate conditions in North and Central America *(31, 32, 43, 44)*. These studies mainly focused on constructing more precise methods for climate prediction; in particular, using the Coupled Model Inter-comparison Project Phase 5 (CMIP5). CMIP5 provides a framework for coordinated climate change experiments. A main goal of the project was to provide projections of future climate change on a near timescale (up to 2035) and long-

term timescale (up to 2100 and beyond), and to evaluate their accuracy by comparing the projections to climate data observed in the short-term past *(33)*.

The Couple Model Inter-comparison Project Phase 5 (CMIP5) includes more than 50 different models that are able to project the past and future climate data. CMIP5 is the newest set of coordinated climate model experiments conducted to provide a multi-model understanding of carbon cycle and clouds, evaluate climate prediction ability on decadal scales, and to determine the reasons that similarly forced climate prediction models lead to various responses *(33)*. Different types of climate scenarios vary based on their atmospheric horizontal resolution and their model types. These models also take the interaction of various natural effects such as oceans, vegetation, and land surfaces into account. It should be noted that these models may not provide appropriate results for every location of interest. Therefore, a proper analysis should be performed to choose the best models for the location of interest. This is achieved by comparing historical results of the adopted climate model to the observed data at the location of interest; which can be performed using the risk quantification framework proposed in this project.

Statistical downscaling is a widely used tool to convert the global scale climate data (e.g., 2 degree scale) to regional scale (e.g., 1/8 or 1/16 degree scale). Several statistical downscaling methods such as bias correction and spatial downscaling (BCSD), constructed analogues (CA), and daily bias correction constructed analogs (BCCA) are available in the literature *(45, 46)*. The BCCA model is a hybrid downscaling method which uses a quantile mapping bias correction on large scale data. This method combines the bias correction and daily downscaling which are typically used separately in other methods. Due to the hybrid performance of BCCA, it was shown to produce more accurate prediction of climate data *(46)*.

Variability in future GHG emission can be modeled in terms of Representative Concentration Pathways (RCPs) *(43)*. Different RCP values consider the change in radiative forcing of GHG from pre-industrial times to the 21st century. Radiative forcing can be described as the difference between absorbed insolation energy and the reflected radiation energy by the earth. Four RCP levels commonly used are RCP 2.6, RCP 4.5, RCP 6, and RCP 8.5, where the number represents the range of radiative forcing values in the year 2100 with respect to pre-industrial years. RCP values are presented with Watts per square meters of earth surface (W/m^2) and their positive value indicates the increase in the net energy gained by earth, which may drive global warming. Accordingly, different RCP values will lead to differences in climate prediction regardless of the adopted GCM and downscaling technique. Therefore, various scenarios of RCPs should be considered to account for the uncertainties associated with the future GHG emission *(47)*.

Global climate modeling is generally a computationally expensive task. This is performed through the general circulation model, which employs Navier–Stokes equations to simulate the interaction of different energy sources (e.g., radiation and latent heat) on land, earth, and oceans. Fortunately, due to the considerable research activity in climate change over the past few decades, meta-data for several GCMs is available in the literature. For instance, the refined daily precipitation and temperature data for the time period 1960 to 2100 with BCCA downscaling method are available through Downscaled CMIP3 and CMIP5 Climate and

Hydrology Projections archive at Brekke et al. *(48)*. The BCCA climate projection covers the North American Land-Data Assimilation System which contains contiguous United States plus portions of southern Canada and northern Mexico, spanning from 25.125° N to 52.875° N and - 124.625° E to -67.000° E. These data sets are used in this study for quantifying the flood hazard at the bridge location.

4.4. Streamflow Prediction

In general, three types of rainfall-runoff models can be used to draw a relationship between climate data and streamflow: metric, conceptual, and physics-based models. While metric models use the observed rainfall and streamflow data to characterize the response of a given basin, conceptual models use internal processes of the basins to describe the storage and movement of water between atmosphere, lithosphere and hydrosphere. In addition, Physics-based models use numerical simulation of equations of motion to characterize the catchment response. Conceptual and physics-based models are generally more involving than metric ones; they require specialized software and can be computationally expensive *(49)*. Several physics-based hydrological models such as variable infiltration capacity (VIC) *(36)*, RAPID *(38)*, and Riverware *(39)* have been developed in recent decades to estimate the response of a basin and the streamflow. In contrast, metric streamflow modeling tools are convenient in drawing a dynamic relationship between basin rainfall and streamflow of a river *(50)*.

This study employs the hybrid conceptual-metric tool IHACRES *(51)* which uses statistical analysis to calibrate a streamflow prediction model and establish a relationship between the observed precipitation, temperature, and streamflow data. This relationship can be used to estimate the streamflow based on future precipitation and temperature profiles obtained from different GCMs. The tool uses a nonlinear module to convert observed rainfall into an effective rainfall and a linear module to convert the effective rainfall to streamflow. The model defines the effective rainfall, U_k as *(52)*:

$$U_k = [c(\phi_k - l)]pr_k \quad [1]$$

with

$$\phi_k = r_k + (1 - 1/\tau_k)\phi_{k-1} \quad [2]$$

and

$$\tau_k = \tau_w \exp(0.062 f (T_r - T_k)) \quad [3]$$

in which c = the mass balance, ϕ_k = the soil moisture index, l = the soil moisture index threshold, p = the nonlinear response term, and r_k = the observed rainfall. τ_k = the drying rate, τ_w = the reference drying rate, f = the temperature modulation, and T_r = the reference temperature, and T_k = the drying temperature. The linear module defines the streamflow Q_k as:

$$Q_k = -\alpha Q_{k-1} + \beta U_{k-\delta} \quad [4]$$

where α = storage coefficient, β = fraction of effective rainfall, and δ = the delay between the rainfall and streamflow. In addition, a second-order transfer function is used to create a unit hydrograph as follows:

$$Q_k = \frac{b_0 + b_1 z^{-1} + b_2 z^{-2}}{1 + a_1 z^{-1} + a_2 z^{-2}} U_{k-\delta} \quad [5]$$

where z = the time-step shifter, a_i , b_i = fitted parameters that are defined based on the type of flow (i.e., quick or slow flow). Finally, the efficiency of the model is evaluated by computing the coefficient of determination that measures the fit between observed and modeled streamflow which is computed as follows:

$$R^2 = 1 - \frac{\sum \left(Q_o - Q_M\right)^2}{\sum \left(Q_o - \overline{Q_o}\right)^2} \quad [6]$$

where Q_o = observed streamflow value and Q_M = modeled streamflow value. Generally, R values greater than 0.75 are acceptable for big basins *(53)*.

4.5. Time-Dependent Scour Prediction

Scour depth is a key variable that significantly affects the time-variant performance of bridges subjected to flood conditions. Scour modeling is a process affected by several sources of uncertainty (e.g., modeling uncertainty and randomness in soil properties, bridge geometry, and river discharge, among others). Local scour at piers is a function of bed material characteristics, bed configuration, flow characteristics, fluid properties, and the geometry of the pier and footing. In the U.S. bridge design and assessment practice, design specifications such as the AASHTO LRFD *(2)* include recommendations for design of bridge piers against scour, which requires this design to be performed on the basis of an approved method for scour predictions. These methods are generally empirical equations with parameters calibrated mostly using experimental flume tests. These equations provide the maximum expected scour depth; the foundations must be placed under this depth to avoid scour failure.

In this project, the scour depth at piers is calculated as *(53)* which was established using a set of flume tests on different soil conditions. The time-dependent scour prediction process starts with identifying the approach velocity V_{appr} representing the water velocity at the location of interest and the pier diameter D. Next, the maximum pier scour at each day Z_{max} is computed as

$$Z_{\max} = 0.18 \times \mathrm{Re}^{0.635} \quad [7]$$

where Re = Reynolds number, given by:

$$\mathrm{Re} = \frac{D \times V_{\max}}{\nu} \quad [8]$$

in which V_{max} = the maximum velocity calculated as $1.5 \times V_{appr}$ and ν = the kinematic viscosity of water (i.e., 10^{-6} m^2/s at 20° Celsius).

Several empirical equations can be used for drawing a relationship between the discharge and water velocity. However, these equations may not be reliable for all locations and channel types. Accordingly, the proposed approach employs a curve fitting technique to establish the relationship between velocity and river discharge. The fitting process is based on the observed velocity and discharge data, at the location of interest, available through the United State Geological Survey database *(54)*.

Finally, the time-dependent scour depth is calculated using multi flood accumulation model proposed in Briaud, et al. *(55)*. This model is suitable for evaluating the time-dependent scour depth in cohesive soils where the equilibrium scour may not be reached during a single flood event. Figure 1 presents the flowchart of the methodology implemented to the establish time-dependent scour depth prediction.

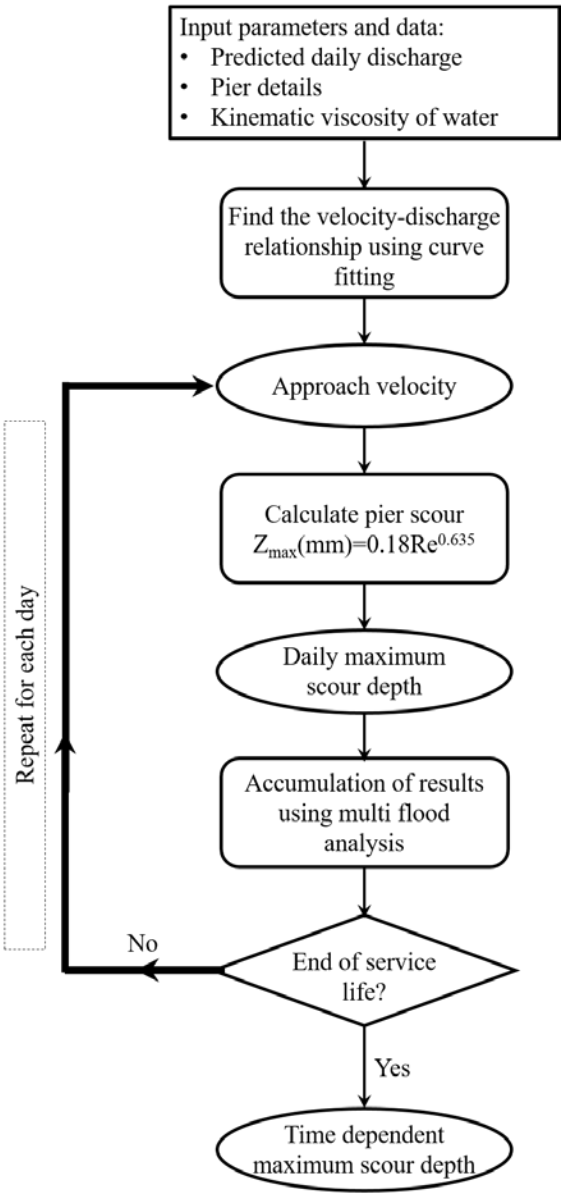

Figure 1. Flowchart of time-dependent scour prediction.

4.6. Capacity of Bridge Foundations

Probabilistic infrastructure management approaches usually involve analytical or numerical structural analysis tasks. Although, numerical approaches (e.g., finite element analysis) are more appealing due to their higher accuracy, they may not be efficient for performing probabilistic analysis. These probabilistic approaches often involve large number of simulations that require executing the numerical models iteratively and can be computationally expensive. Accordingly, in this project, the structural capacity is modeled using analytical models. The adopted formulation for quantifying the capacity of bridge foundation has been found to provide reliable results when compared to the results of the experimental investigations *(56)*.

Although the proposed risk assessment approach is equally applicable to different types of bridge foundation, this project focuses on the capacity of pile foundations with steel H-piles. Lateral and axial limit states are considered to evaluate the behavior of this foundation type under horizontal and vertical loads. The ultimate lateral load carrying capacity H_L of one pile is *(56)*:

$$H_L = 0.3\left(\eta K_P^2 + \xi K \tan\delta\right)\gamma a B(2.7a - 1.7L) \quad [9]$$

with

$$a = \frac{-\left(0.567L + 2.7e\right) + \left(5.307L^2 + 7.29e^2 + 10.541eL\right)^{0.5}}{2.1996} \quad [10]$$

where η = shape factor to account for the non-uniform distribution of earth pressure, K_p = passive earth pressure coefficient, K = lateral earth pressure coefficient, δ = interface friction angle between the pile and the soil, γ = effective unit weight of soil, a = depth to the point of rotation, B = diameter or width of the pile, L = embedded length of pile, and e = eccentricity of loading. In this model, shear resistance contribution from both the front soil and side soil is considered. In order to evaluate the capacity of each pile in the pile group, a reduction factor is applied to the capacity of a single pile *(57)*. An equivalent circular diameter of H-pile is computed based on Reese and Van Impe *(58)*.

The ultimate axial load carrying capacity R_v is expressed as a sum of shaft resistance and toe resistance of a pile as:

$$R_V = R_s + R_p \quad [11]$$

$$R_s = f_s A_s \quad [12]$$

$$R_p = q_p A_p \quad [13]$$

where, R_s = the shaft resistance and R_p = the toe resistance of the piles. f_s = unit shaft resistance over the pile surface area, A_s = pile shaft surface area, q_p = unit toe resistance over the pile toe area, and A_p = pile toe area.

4.7. Bridge Risk Analysis

In this approach, bridge piers are subjected to traffic live loads and dead loads computed using the AASHTO LRFD Bridge Design Specifications *(59)*. The adopted HL-93 live load model consists of the worst combination of the design truck plus design lane load or a design tandem plus design lane load. In addition, flood-induced lateral load F_L acting on bridge pier is calculated as *(60)*:

$$F_L = p \times A \quad [14]$$

With

$$p = C_D \frac{\gamma}{2g} V_{appr}^2 \quad [15]$$

where A = area of accumulated debris, p = water pressure on piers, C_D = drag coefficient, and V_{appr} = velocity of stream flow.

The load effects and load carrying capacity, performance functions are defined as:

$$G_L(t) = R_L(t) - F_L(t) \quad [16]$$

$$G_V(t) = R_V(t) - F_V(t) \quad [17]$$

where $G_L(t)$ = lateral performance functions at time t, $G_V(t)$ = the vertical performance functions at time t, $H_L(t)$ = respective time-variant lateral capacity, $R_V(t)$ = the respective time-variant vertical capacity, $F_L(t)$ = respective lateral load effects at time t, and $F_V(t)$ = the respective vertical load effects at time t. These performance functions are used to evaluate the probability of failure and risk due to flood and flood-induced scour.

In order to assess the failure probability of a bridge foundation considering the time-variant scour under climate change, Monte Carlo Simulation (MCS) of the scour model, given by equation 7, is conducted in MATLAB environment *(61)*. This process uses the climate-based generated streamflow hydrographs and is used to draw samples from the scour depth at any time instance in the future given the climate scenario (i.e., for a certain GCM, downscaling method, and RCP value). The probability distribution function (PDF) of the time-variant lateral and axial capacity of the piles (given by Equations 9 and 11, respectively) can be obtained using the simulation process. Next, the PDF of the time-variant flood loads are obtained from the generated climate-based river streamflow.

The PDFs of the time-variant capacity and load effects are next used within the MCS to obtain the point-in-time probability of failure of the bridge pier as:

$$P_f(t) = P[any \quad g_i(t) < 0] \quad [18]$$

where $P_f(t)$ = point in time probability of failure and $g_i(t)$ = the I th performance function. The failure probability is computed as the failure probability of a system with failure modes

connected in series. The cumulative annual probability of failure, representing the cumulative distribution function (CDF) of the time to failure, is computed as *(21)*:

$$TDP(y) = \sum_{i=1}^{t}\left(P_{f,i}\prod_{j=1}^{i}\left(1 - P_{f,j-1}\right)\right) \quad [19]$$

where $TDP(y)$ = cumulative annual probability of failure and P_f = point-in-time annual failure probability of the piles. The risk of structural failure is established based on evaluated consequences as:

$$Risk(t) = TDP(y) \times C \quad [20]$$

where $Risk(t)$ = the time-dependent risk, C = the monetary value associated with bridge failure and calculated considering rebuilding cost C_{reb}, running cost C_{run}, and time loss C_{tl} due to the bridge failure and road closure. This approach provides a mechanism for integrating sustainability metrics by computing the monetary value associated with social and environmental impacts. All of the costs are calculated in terms of U.S. dollars (USD) as *(62)*

$$C = C_{reb} + C_{run} + C_{tl} \quad [21]$$

where the rebuilding cost (C_{reb}) is estimated as a function of bridge area considering the length and width of the bridge. In some cases, only some parts of the structure need to be repaired or replaced, therefore, this consequence is also known as repair cost and is calculated as follows:

$$C_{reb} = C_{rc} W_b L_b \quad [22]$$

in which C_{reb} = rebuilding cost ($) per unit area, W_b = bridge width (m), and L_b = bridge length (m). The running cost represents the additional expenses encountered through vehicle operation on the detour due to bridge closure and it is calculated as:

$$C_{run} = C_{rv} DADTd \quad [23]$$

where C_{rv} = average cost of running vehicle ($/km), D = detour length (km), ADT = average daily traffic affected by bridge closure (vehicles/day), and d = duration of detour (days).

The time loss cost C_{tl} represents the loss of time per passenger for traveling through the detour. This cost is calculated as:

$$C_{tl} = \left[C_1 O\left(1 - \frac{T}{100}\right) + C_2 \frac{T}{100}\right]\frac{DADTd}{S} \quad [24]$$

in which C_1 = value of time per adult ($/hr.), C_2 = value of time for truck ($/hr.), S = average detour speed (km/hr.), T = average daily truck traffic (%), and O = occupancy rate. The flowchart of the risk analysis framework proposed in this project is shown in Figure 2.

The proposed framework contains four main modules: (a) flood prediction using climate modeling, (b) time-dependent scour prediction, (c) structural performance prediction considering floods and flood-induced scour, and (d) estimation of failure probability, failure

consequences, and time-dependent risk profile. As the first step of this framework, suitable global climate models for the region of interest should be selected along with associated downscaled precipitation and temperature profiles. Next, the discharge at the bridge location should be calculated using streamflow modeling techniques. This is performed herein through a hybrid conceptual-metric model which uses the historical records to establish a relationship between river discharge and precipitation and temperature patterns. The resulting river discharge profiles are then used to assess the scour propagation and structural performance. Next, the probability of bridge failure is computed using probabilistic simulations of the bridge performance function in terms of the resistance and load effects. The last module of this framework is focused on estimating the consequences of bridge failure and generating the time-dependent risk profile. As depicted in Figure 2, the proposed framework can identify the risk of bridge failure considering climate change. In this report, the framework has been applied to a steel girder bridge, However, the framework can be applied to different bridges with various soil properties (clay, sand, etc.), scour types (pier scour, contraction scour, etc.), and structural systems.

Figure 2. Flowchart of the performed probabilistic analysis.

4.8. Time-Dependent Marine Corrosion

Evaluating the long-term behavior of structures subjected to a corrosive environment is highly dependent on estimating the material loss. Due to the significant uncertainties associated with the factors associated with the time-dependent corrosion loss models, predicting the residual capacity of structural components under corrosion should be performed probabilistically.

In addition, adopting historical climate records may lead to errors in characterizing the corrosion loss prediction parameters (e.g., water temperature). Therefore, the proper selection of corrosion model parameters should consider uncertainties and long-term climate change. In this section, the immersion corrosion model presented by Melchers *(63, 64)* is used to model corrosion loss in steel structures. The long-term effect of elevated nutrient concentration considering climate change can be addressed using this model.

The historical water and air temperature, dissolved inorganic nitrogen (DIN), and the predicted air temperature profiles from GCMs are the inputs of this corrosion prediction model. Since climate modeling only provides air temperature prediction, water temperature profiles are established based on a curve fitting technique that can draw a relationship between the air and water temperatures. In addition, distribution fitting is employed to obtain the best probability density function (PDF) which fits the DIN data adopted from USGS water data database *(54)*. Random DIN values are then generated through random sampling techniques to conduct the probabilistic simulation. The resulting DIN values along with the predicted future water temperature profiles are then used to estimate the y-intercept at time zero (C_s) and the slope of the long-term corrosion rate (R_s) of the adopted corrosion loss prediction model described by Melchers *(64)*. This process results in time-dependent corrosion loss curves considering the annual variation of temperature due to climate change. The Flowchart of the proposed corrosion prediction approach is shown in Figure 3.

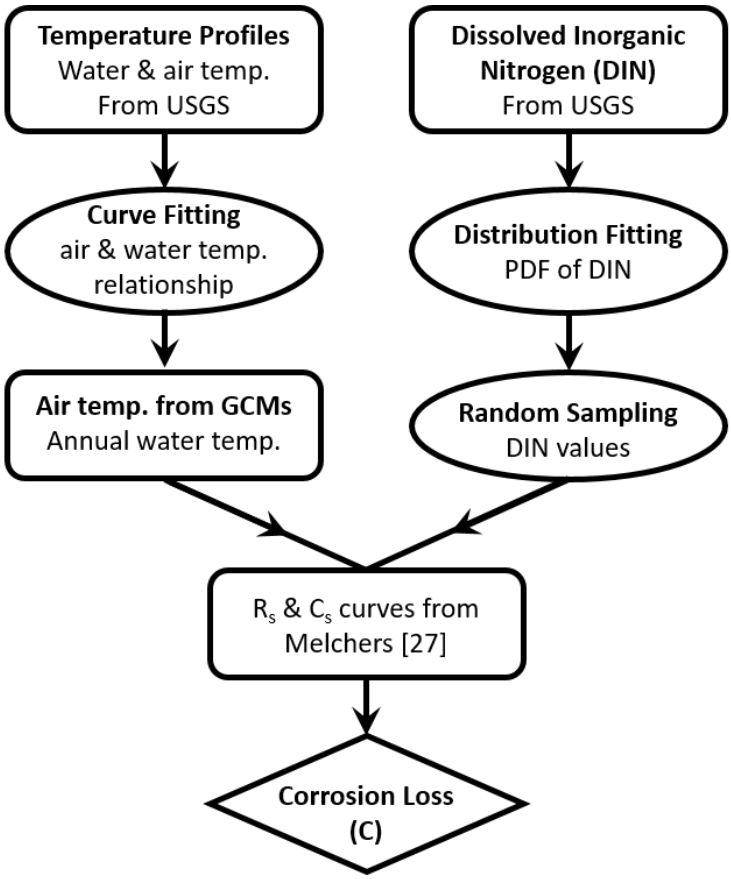

Figure 3. Flowchart of corrosion loss prediction.

4.9. Time-Dependent Fresh Water Corrosion

The previously discussed immersion corrosion approach is applicable to bridges located in a marine environment, this corrosion model may not accurately predict the corrosion loss for the freshwater cases. Eurocode 3, part 5 has presented the corrosion loss prediction data for freshwater cases. These values are adopted and presented through Table 1.

Table 1. Euro code recommended value for the corrosion loss of piles in fresh water.

Required Design Working Life	5 years	25 years	50 years	75 years	100 years
Common fresh water (e.g. rivers) in the zone of high attack	0.15 mm	0.55 mm	0.9 mm	1.15 mm	1.4 mm
Very polluted Freshwater (e.g. sewage) in the zone of high attack	0.3 mm	1.3 mm	2.3 mm	3.3 mm	4.3 mm
Seawater in temperate climate in the zone of high attack (low water and splash zones)	0.55 mm	1.9 mm	3.75 mm	5.6 mm	7.5 mm
Seawater in temperate climate in the zone permanent immersion or in the intertidal zones	0.25 mm	0.9 mm	1.75 mm	2.6 mm	3.5 mm

4.10. Combined Effects of Flood, Flood-Induced Scour, and Corrosion

The time-dependent risk profile under flood and flood-induced scour considering climate change effects can be achieved using the proposed flowchart in Figure 3. Adopting global climate models and streamflow modeling, time-dependent scour prediction, structural performance evaluation and evaluating the consequences of bridge failure are among the most important steps of this probabilistic framework. Figure 4 visualizes this framework.

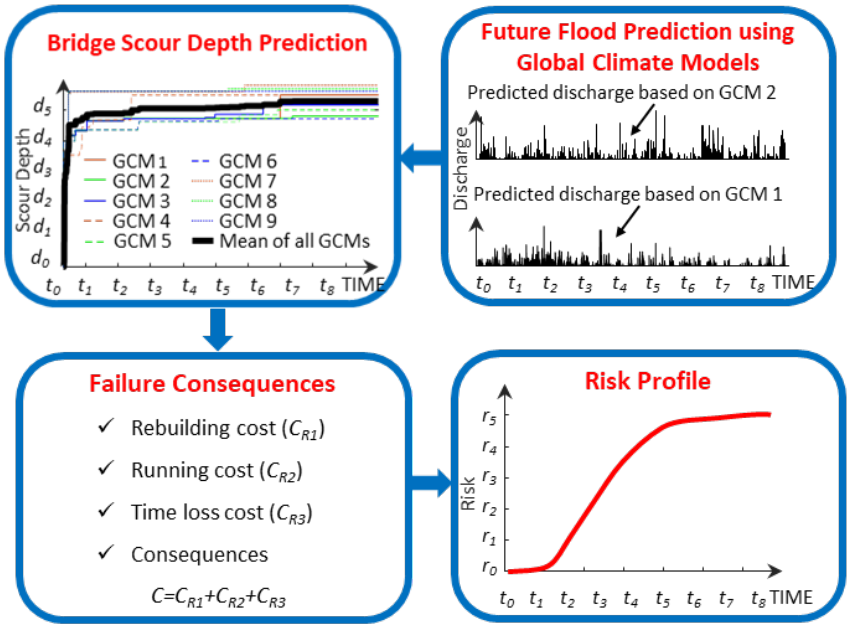

Figure 4. Visualized framework under flood and flood-induced scour.

The effect of corrosion propagation can be also integrated in this framework. This can be achieved by either of the marine corrosion or freshwater corrosion approaches. In the case of marine corrosion, the effects of climate change on future temperature prediction can be also included. A visualized framework for risk assessment under flood, flood-induced scour, and corrosion deterioration considering climate change effects is presented in Figure 5.

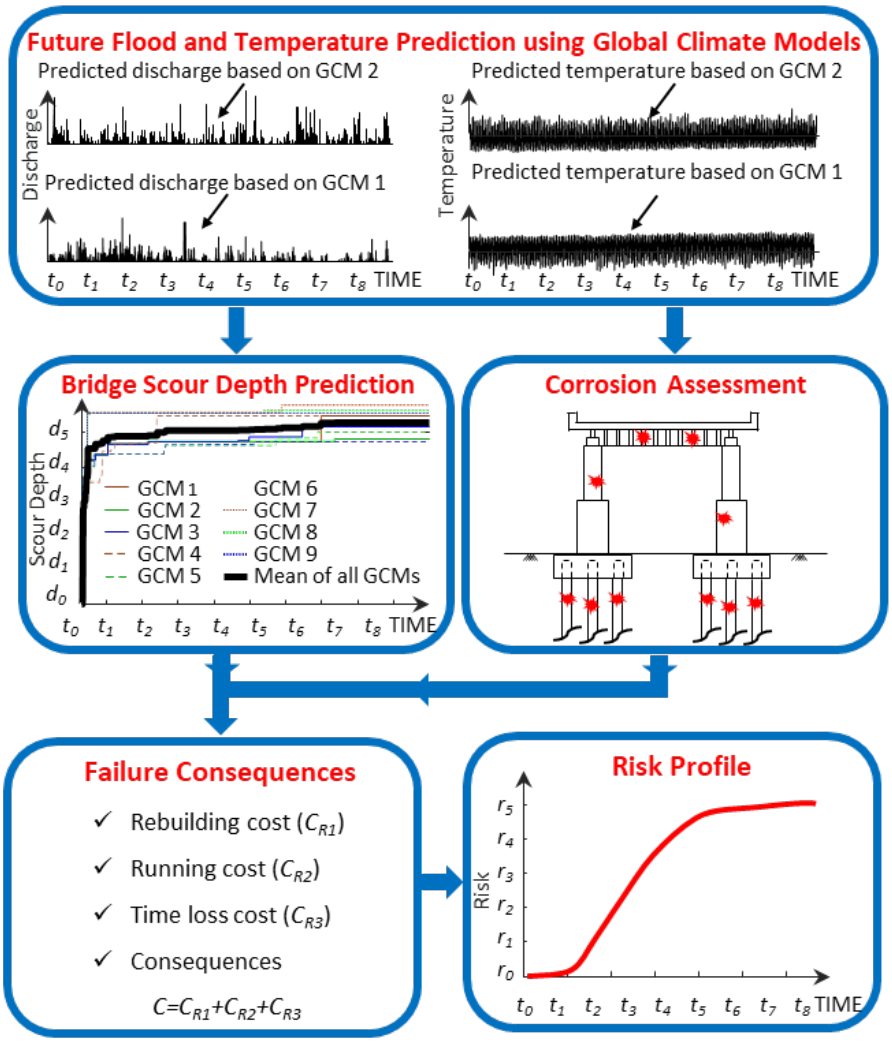

Figure 5. Visualized framework under flood, flood-induced scour, and marine corrosion.

4.11. Optimization of Bridge Management Activities

The proposed framework can be also expanded to a risk-based probabilistic framework for optimizing the maintenance planning of bridges. Such framework can be used to establish the optimum maintenance and retrofit activities which can extend the service life and reduce the failure risk with lowest possible life-cycle cost. Such approach is capable of performing the optimization for bridges under flood, flood-induced scour, corrosive environment, and earthquake hazards. The process is performed through four main modules: (a) flood and temperature prediction using climate modeling, (b) structural performance prediction considering floods, flood-induced scour, corrosion, and earthquake hazards in the super- and sub-structures, (c) consequences and risk estimation, and (d) maintenance optimization and management strategies.

The last step of this framework is focused on optimization of the of the management activities using the established risk profiles of the investigated bridge and the available maintenance, retrofit, or repair procedures. In this step, various intervention options for the predicted damage

states should be analyzed with their respective costs. Next, the management objectives and constraints are defined and the optimization is performed to establish the optimum management plans. A layout of such optimization framework is presented in Figure 6. An approach for identifying optimum repair, maintenance, and/or retrofit activities required to improve the sustainability of bridges constructed in a multi-hazard environment is presented. The procedure of this framework starts with quantifying the increase in the bridge failure risk during flood events considering the expected change in climate conditions. Climate scenarios extracted from global climate models that are appropriate for the location of interest, along with different carbon emission scenarios, are used to predict future climate trends. The predicted temperature, streamflow, and time-dependent scour depths based on these climate scenarios are then integrated in a probabilistic framework to perform multi-hazard risk analysis considering flood, scour, and corrosion hazards. Probabilistic simulation enables establishing a multi-hazard risk profile for the structure of interest. Probabilistic simulations also assist in accounting for the uncertainties associated with hazard occurrence, load effects, and structural resistance. Multi-objective optimization can be used next to establish the best intervention schedules required to fulfill the management needs.

The developed framework of this study could be implemented by bridge officials to manage the existing stock of deteriorating bridges while reduces the associated life-cycle cost and maintain the desired performance level throughout the service life of bridges. In particular, the proposed framework can provide a better understanding of the system performance under multiple hazards. Accordingly, bridge managers can take corrective actions to prevent structural failures under extreme events. This will eventually improve the durability and extend the service life of existing bridge infrastructure and subsequently reduce the economic and social consequences of the bridge failure. In addition, the results of this study can be used for real-time decision-making for traffic control during natural disasters or disaster evacuation operations. Therefore, using the results of this project, a better budget allocation and significant societal, environmental, and economic benefits can be achieved and unnecessary expenditures on infrastructure management can be avoided.

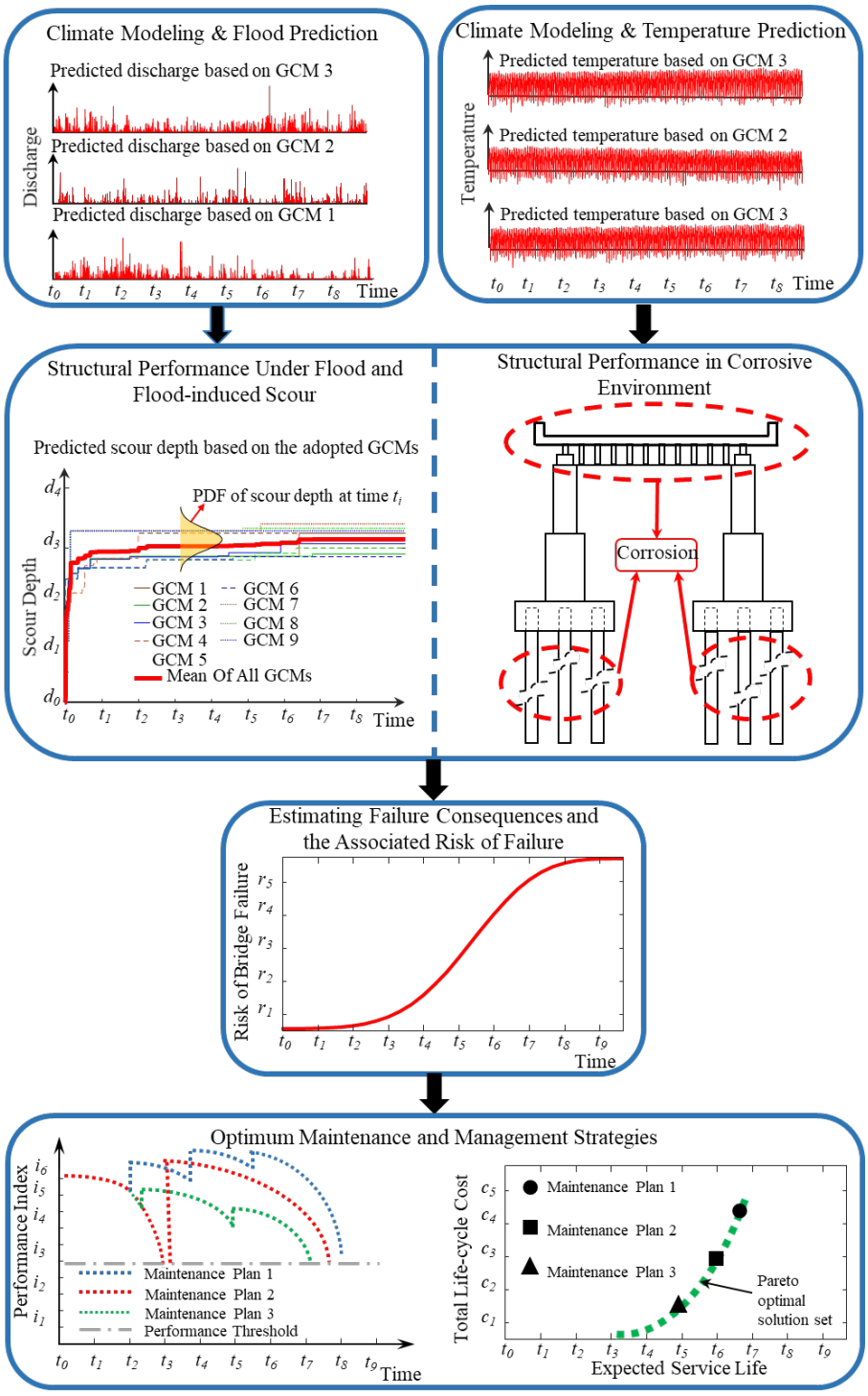

Figure 6. Proposed framework for maintenance optimization of the bridges.

5. FINDINGS

The presented framework is illustrated on the South Bound I-35 Bridge over the Red River. The bridge serving a major freight route linking Southern and Northern US states is located on the Oklahoma-Texas border. During the past few decades, the Red River has experienced several heavy floods which caused significant damage to surrounding areas. The most recent severe flood occurred in May 2015, in which the water reached the level of the superstructure. In addition, several other bridges along the Red River basin experienced partial or total failure during this flood *(6, 7)*. The I-35 bridge represents an ideal example due to its strategic location on a major freight route, the aggressiveness of flooding conditions on the Red River, the large daily traffic utilizing the bridge, and the lack of alternative routes in case of bridge failure.

5.1. Case Study

This bridge accommodates an average daily traffic of 19,800 vehicles with 36% average daily truck traffic *(67)*. The I-35 bridge superstructure consists of five plate girders supporting a reinforced concrete deck, while the substructure is composed of multiple piers supported by steel H-piles (Figure 7a). The bridge is 118.3 m long and 9.5 m wide, with two traffic lanes. The bridge has 11 piers and 32.3 *m* long spans. Since not all the characteristics of the bridge could be obtained, some assumptions related to dimensions were placed. These include the thickness of the concrete deck (35 cm) and the width of the bridge piers (1.2 m). Based on the original construction drawings, the riverbed level is considered to be 10 m below the deck. In this study, the failure risk analysis has been performed considering a single pier. However, system analysis covering all the piers can be performed using series-system reliability formulation. A layout of the bridge pier with pile configuration is shown in Figures 7b and 7c. The studied bridge pier has two groups of 9 steel H-piles (HP 12x53 steel piles), each is 11.2 m long. Piles are aligned such that their strong axis is perpendicular to the direction of streamflow.

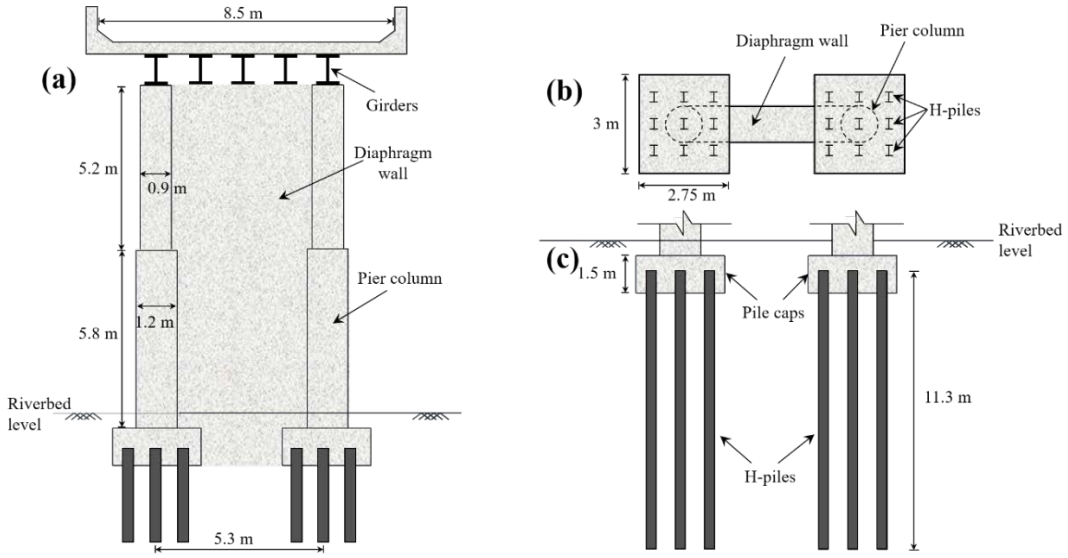

Figure 7. Layout of bridge pier with pile configuration (a) piers and superstructure (b) plan view of pile caps (c) side view of pile caps and H-piles.

5.1.1. Climate Modeling and Flood Prediction

The downscaled climate data for MPI_ESM_LR, CCSM4, and MIROC5 global climate models downscaled using BCCA method with RCP 2.6, RCP 4.5, and RCP 8.5 are adopted from *(48)*. The precipitation and temperature during the time window ranging from 1960 to 2100 is utilized. These selected GCMs were shown to provide reliable climate predictions for the location of interest *(40)*. The combination of three GCMs and three RCP values results in nine different climate data sets. Table 2 shows the detailed information on the adopted climate scenarios. The precipitation and temperature datasets are next used for streamflow prediction using IHACRES *(51)*.

For the I-35 Bridge, the observed precipitation, temperature, and streamflow time-histories corresponding to the period of 2000-2015 are imported to the IHACRES for evaluating the accuracy of the prediction model. The observed streamflow datasets are adopted from the United State Geological Survey station on the Red River near Gainesville, TX (USGS ID: 07316000) *(54)* located 300 m upstream of the bridge. The observed temperature and precipitation data are acquired from NOAA dataset *(5)* for the same time period. With an area of almost 70,000 km^2 and 2200 km in length, the climate data within the Red River basin is subject to considerable variability due to the large basin size. Accordingly, the observed temperature and precipitation time-histories for 30 stations located throughout the basin are analyzed and their average time-histories are used as the input data for the river flow prediction.

Table 2. Adopted climate models for the investigated I-35 bridge.

Modeling Center (or Group)	Institute ID	Model Name	RCP (W/m^2)	Resolutions	Datasets
National Center for Atmospheric Research	NCAR	CCSM4	2.6 4.5 8.5	1/8 degree	Max. temp. Min. temp. Precipitation
Atmosphere and Ocean Research Institute (The University of Tokyo), National Institute for Environmental Studies, and Japan Agency for Marine-Earth Science and Technology	MIROC	MIROC5	2.6 4.5 8.5	1/8 degree	Max. temp. Min. temp. Precipitation
Max-Planck-Institut für Meteorologie (Max Planck Institute for Meteorology)	MPI-M	MPI-ESM-LR	2.6 4.5 8.5	1/8 degree	Max. temp. Min. temp. Precipitation

Selection of the calibration period for climate prediction is related to the application of the model, if the model applies to flood peaks, then the calibration period should contain enough flood peaks to attain proper model calibration. In case of humid catchments, a two- or three-year calibration period is appropriate, while in arid or semi-arid areas a longer calibration period is usually needed *(49)*. For the location of interest in this study, a five-year calibration period from September 2004 to August 2009 is selected. The linear and nonlinear modules are used to draw a relationship between the observed rainfall and streamflow. The predicted data has a monthly R^2 value of 0.82 which meets the minimum recommended values *(51)*. Figure 8

shows a comparison between observed and modeled streamflow data from 2000 to 2016. As shown, a reasonable agreement between the observed and predicted data is achieved.

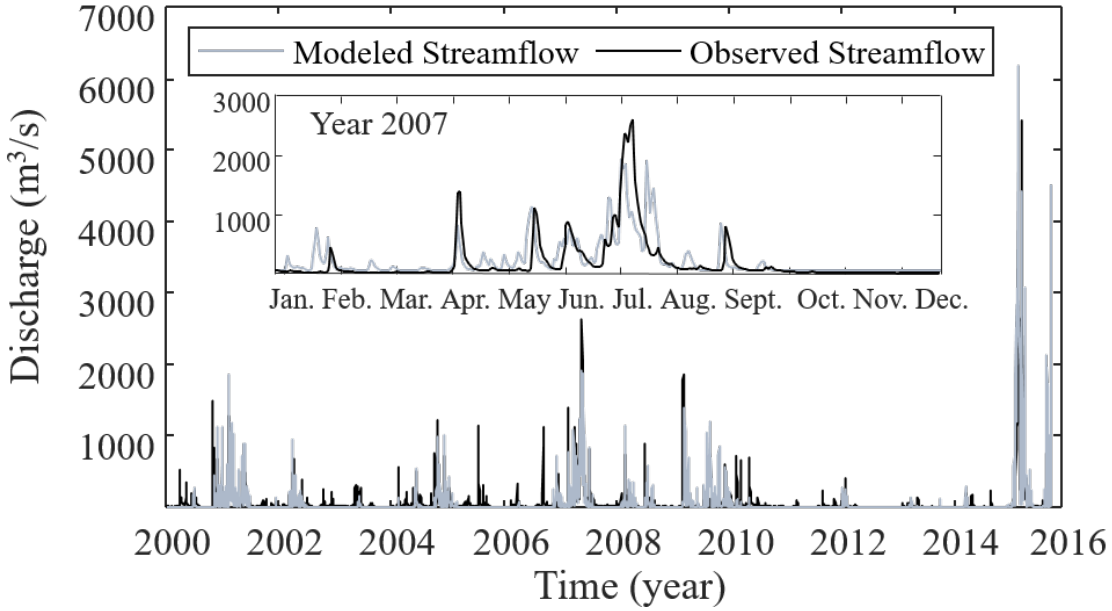

Figure 8. A comparison between observed and the modeled streamflow data (calibration period Sep. 2004 to August 2008).

After the calibration process, the downscaled temperature and precipitation datasets for the analyzed 30 stations are used and their average is calculated. These average values associated with each of the nine climate scenarios (defined by different combinations of GCMs and RCPs) are used for predicting the streamflow. Next, the streamflow time-history associated with each climate scenario for the period of 1960 to 2099 is established using the achieved calibration parameters. Figures 9a, b, and c show the average precipitation, average temperature, and the predicted streamflow time series for CCSM4 model with RCP 2.6, respectively.

The analysis of predicted streamflow resulting from the considered climate models for the location of interest indicates that although the mean annual discharge during the period 1960 to 2100 is decreasing, the maximum annual discharge shows a steady increase. Figure 10a shows the annual discharge versus time for all of the adopted GCMs; additionally, it shows the mean and maximum annual discharge values, respectively. Figure 10b shows only the annual maximum and mean discharge in addition to the linear fit of these two profiles. The figure shows a clear trend indicating a decrease in the overall annual mean discharge. However, as indicated by the linear fit of the discharge peaks, the chance of having larger precipitation events is increasing. This highlights the importance of proper climate modeling during bridge risk assessment.

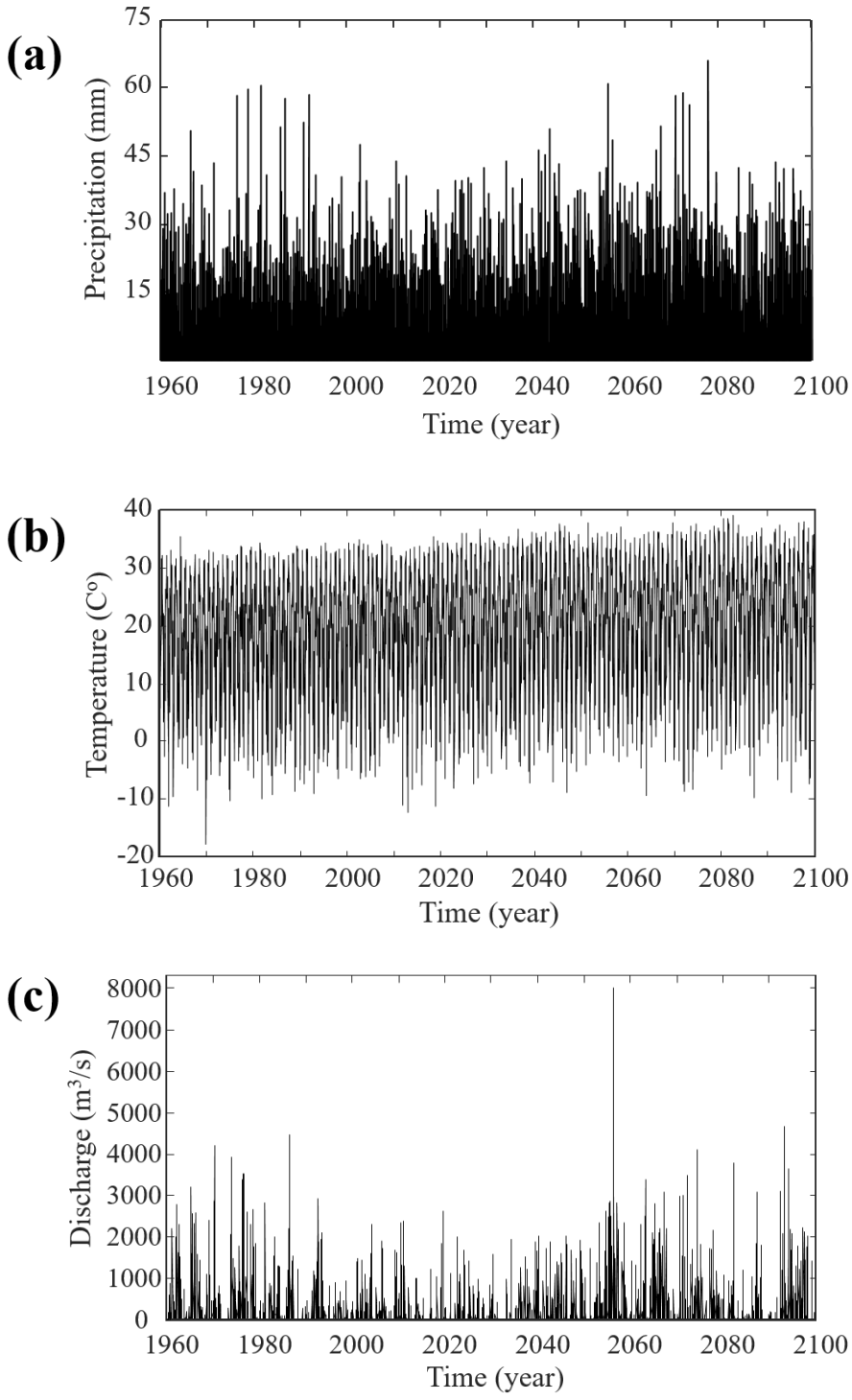

Figure 9. Average daily (a) precipitation, (b) temperature, and (c) streamflow based on CCSM4 model with RCP 2.6.

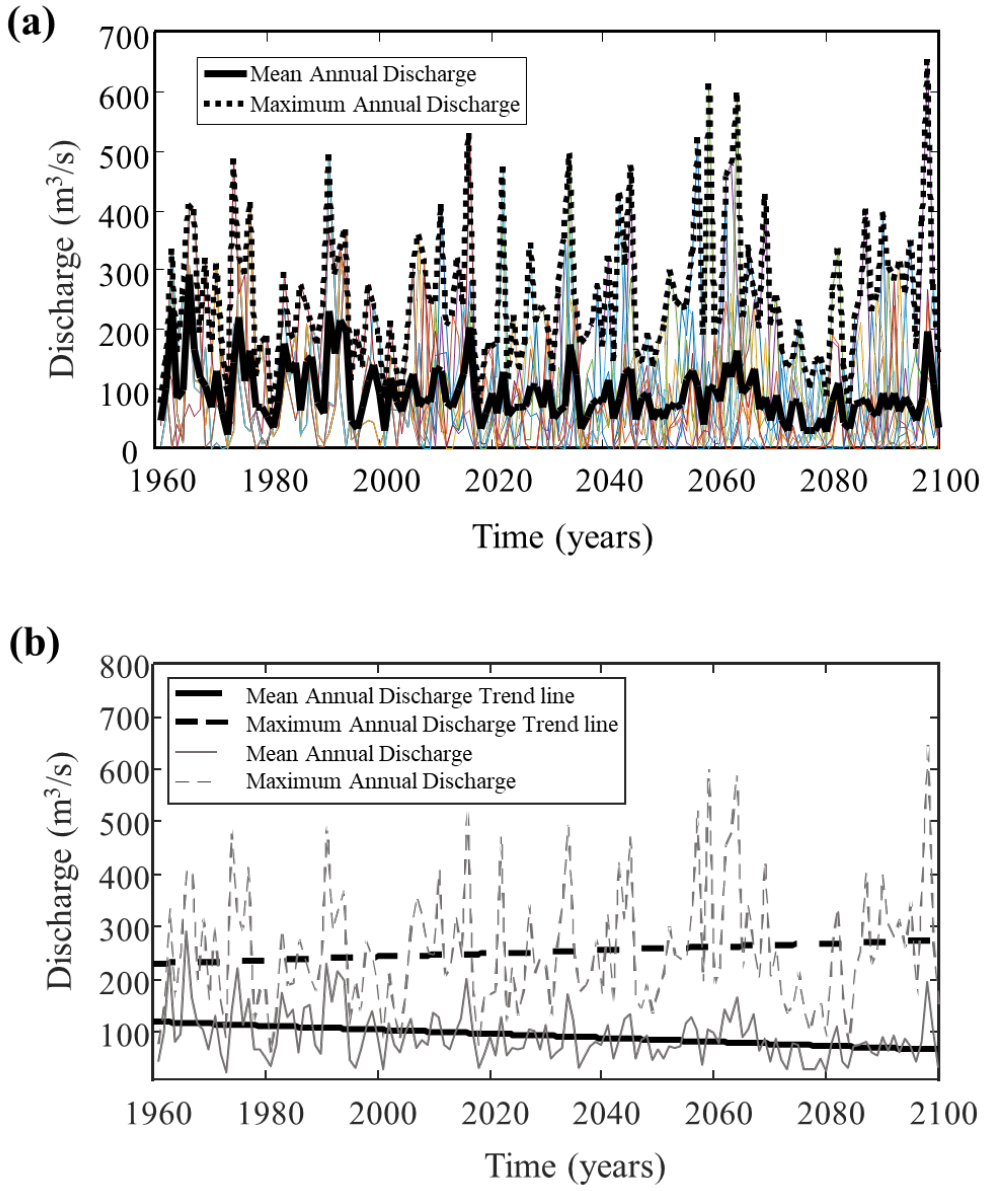

Figure 10. (a) Average streamflow associated with all of the adopted GCMs (b) the trend lines of maximum and average annual streamflow.

5.1.2. Scour Prediction and Risk Assessment

Scour modeling for each streamflow time-series, corresponding to a given climate scenario, is performed using Equation 7. This model requires the velocity as an input parameter. In order to establish a relationship between the velocity and discharge at the bridge location, a curve fitting technique using MATLAB curve fitting toolbox *(61)* is utilized in this project. Figure 11 shows the results of this process.

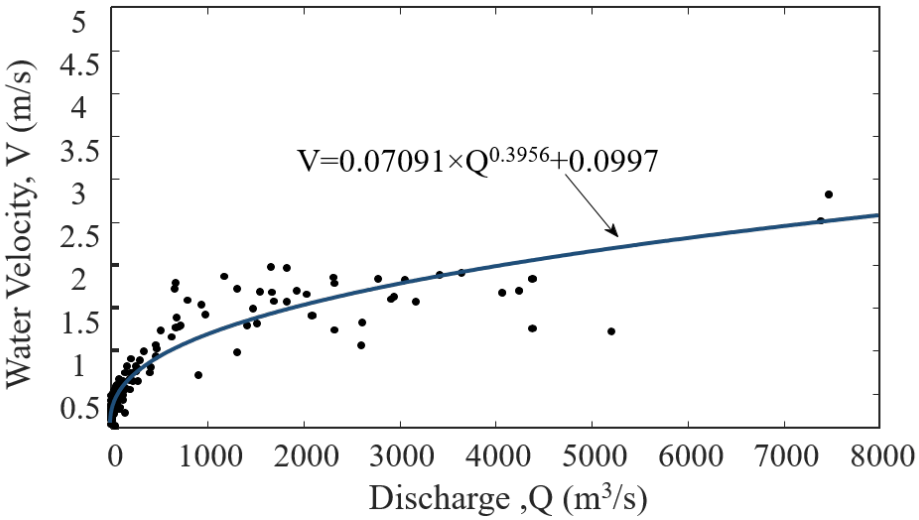

Figure 11. Fitting curve for discharge and velocity.

Time-dependent scour depth associated with different climate scenarios is then established. Figure 12 shows the time-dependent scour depth profiles for all climate scenarios. As shown, there is a considerable variability in the scour depths among the considered scenarios. The results depict up to 30% difference in final scour depth between different climate datasets. This highlights the significant uncertainty associated with the scour prediction considering climate change and justifies the need for probabilistic analysis.

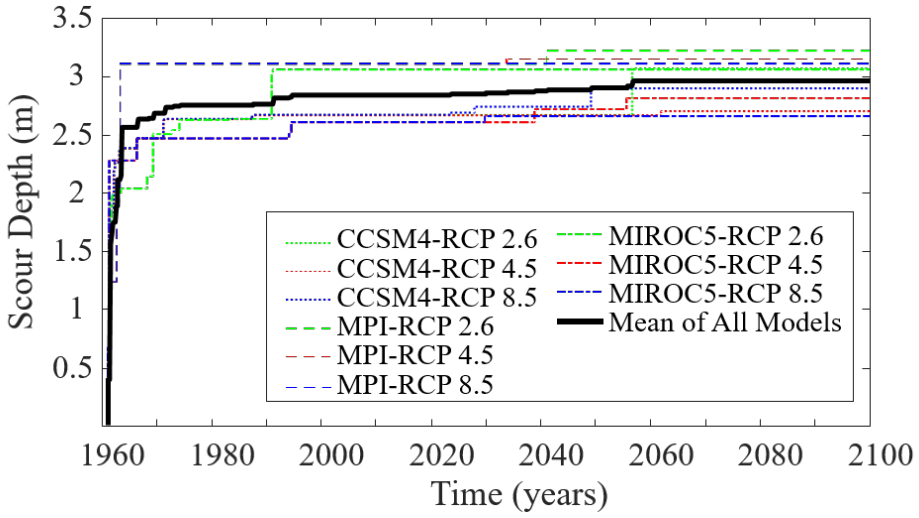

Figure 12. Time-dependent scour depth results based on different GCMs.

In order to consider this variability in the risk assessment, Monte Carlo simulation with 100,000 samples is used to draw samples from the time-variant scour depth at the investigated bridge pier. Next, each sample from the distribution is used to perform the time-dependent scour depth prediction. The internal friction angle of soil is considered as a random variable that follows a normal distribution with mean value of 36° and standard deviation of 1.33 *(68)*. The unit weight of saturated soil is assumed 124 lbs /ft^3, and coefficient of lateral earth pressure is assumed 0.4. In addition to soil parameters, the streamflow is treated as a random variable.

A probabilistic investigation is performed in order to establish the appropriate distribution parameters of the peak annual flow at the location of interest. A peak extraction analysis performed using MATLAB *(61)* is carried out to isolate the peaks within each year. The best distribution type that fits the annual peaks is found as shown in Figure 13. In this specific case study, the exponential distribution fits best the annual peak data. The predicted streamflow of each year is used to predict the parameter of the exponential distribution and the Monte Carlo simulation is used to find the annual histograms of the time-variant scour depth. The probabilistic scour depth is next used to calculate probability of failure using the performance functions given by Equations 16 and 17.

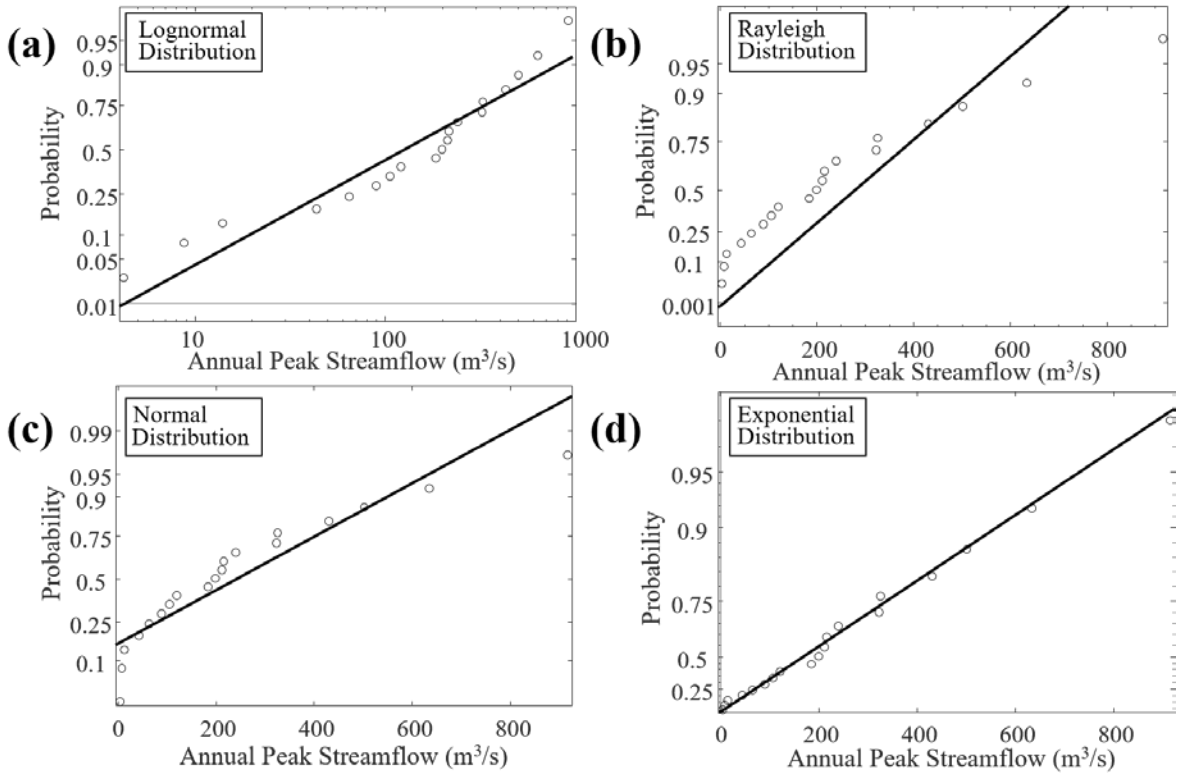

Figure 13. Probability plots of annual peak streamflow using (a) Lognormal (b) Rayleigh (c) Normal (d) exponential distributions.

Axial and vertical load capacity of the piles are calculated using Equations 11 and 12. The shape factors η and ξ associated with the H-piles are assumed 1.0 and 2.0, respectively *(58)*. Figure 14 shows the probabilistic time-variant capacity of the piles in lateral and axial directions. In addition, the PDFs of resistance at the years 2000, 2030, and 2060 are shown in the figure. It is shown that reduction in the lateral capacity reaches 50% at the end of the service life while the maximum reduction in axial capacity is 30%. Vertical loads from traffic and dead load of the structure are calculated based on AASHTO LRFD Specifications *(59)* considering HL-93 loading to obtain maximum vertical forces on the bridge supports. Lateral load due to discharge is calculated using Equation 14. With the probabilistic load and capacity terms in the limit state functions identified, the annual probability of failure can be obtained using the Monte Carlo simulation results.

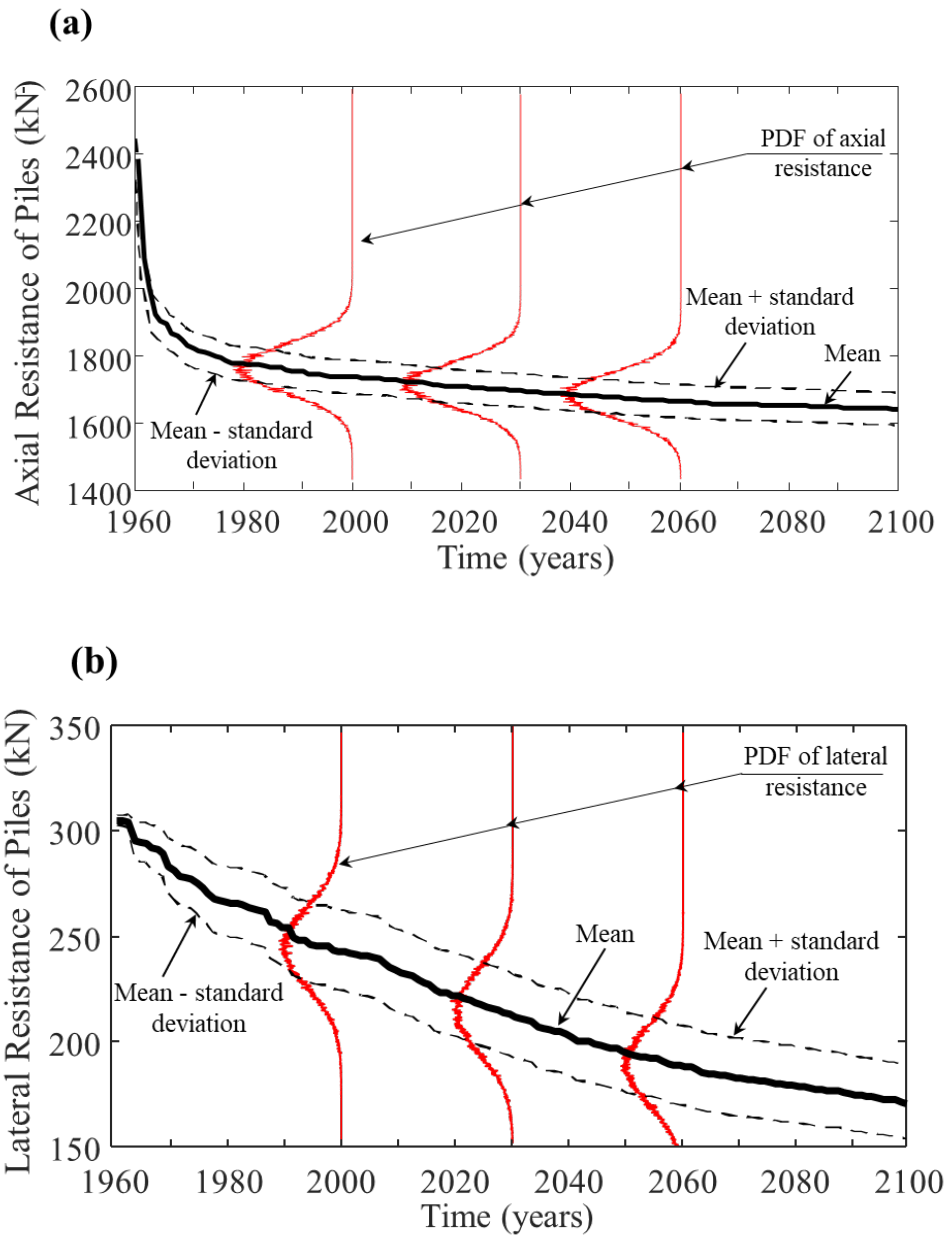

Figure 14. Time variant resistance of piles in (a) axial (b) lateral directions.

After establishing the failure probability profiles, consequences due to bridge failure are evaluated considering repair cost, running cost, and time loss cost, calculated using Equations 2),(2), and(2), respectively. The failure risk is then computed using Equation 20. All the parameters used in calculating the consequences are considered random variables, except the detour length (D) and the duration of the detour (d). Table 3 presents the values of deterministic parameters and the descriptors of randomly distributed parameters used in calculating the failure risk.

In this study, it is assumed that the effect of inflation negates the money interest; accordingly, the discount rate of money is assumed to be zero. The detour length is derived by analysis of

the transportation network to which the bridge belongs. The area on the I-35 before and after the bridge is analyzed to identify alternative routes in case of bridge failure. The analysis indicates that the average travel time is 25 minutes with the intact bridge, while the detour will result in an average of 60 minutes travel time in case of bridge failure.

Table 3. Parameters for evaluation of rebuilding, running, and time-loss costs.

Parameter	Notation	Value	Probabilistic Parameters	References
Rebuilding cost ($/m^2)	*Crc*	\$894 / m^2	Lognormal, *COV*= 0.2	Deco & Frangopol *(21)*
Average cost of running vehicle ($/km)	*Crv*	\$0.08 / km	Lognormal, *COV* = 0.2	Deco & Frangopol *(21)*
Detour Length	*D*	90 km	Deterministic	Estimated based on analysis of traffic network
Average Daily Traffic	A_{DT}	19,800 vehicles/day	Lognormal, *COV* = 0.2	FHWA *(67)*
Duration of detour	*d*	182.5 days (6 months)	Deterministic	Assumed
Cost of time per adult ($/hr.)	*C1*	\$22.82	Lognormal, *COV* = 0.15	Deco & Frangopol *(21)*
Cost of time for truck ($/hr.)	*C2*	\$26.97	Lognormal, *COV* = 0.15	Deco & Frangopol *(21)*
Average detour speed (km/hr.)	*S*	64	Lognormal, *COV* = 0.15	Deco & Frangopol *(21)*
Average daily truck traffic	*T*	36%	Lognormal, *COV* = 0.2	FHWA *(67)*
Occupancy rate	*O*	1.5 adults	Lognormal, *COV* = 0.15	Deco & Frangopol *(21)*

In order to compute the failure probability and risk, Monte Carlo simulation with 100,000 samples is adopted. Figure 15a shows the mean point in time probabilities of failure for all climate models while Figure 15b shows the mean, mean plus one standard deviation, and mean minus one standard deviation of time-dependent risk profile.

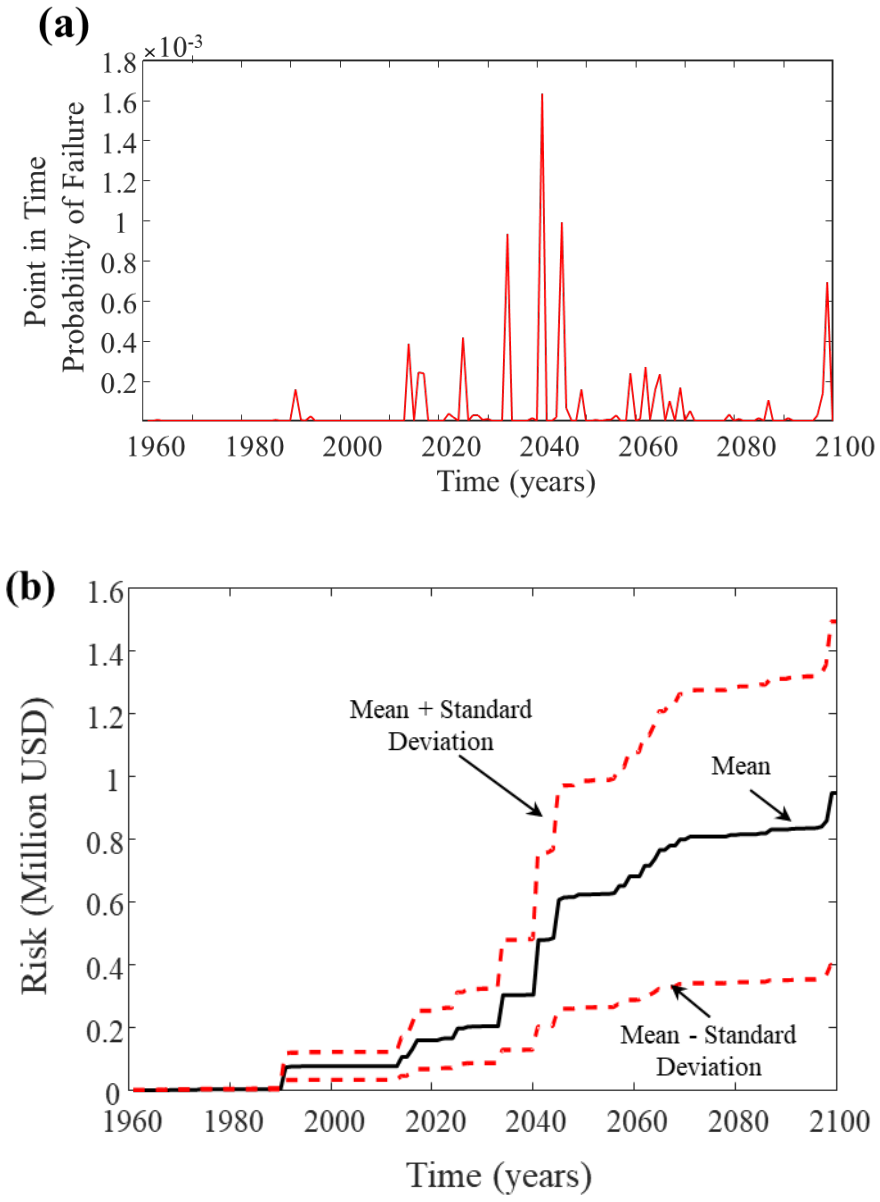

Figure 15. The mean value of (a) point in time probability of failure (b) time-dependent risk based on all climate models.

5.2. Impact of Climate Change on Bridge Failure Risk

Since one of the main goals of the project is to evaluate the impact of climate change on the risk profile of a given bridge, the risk profile resulting from the proposed approach considering climate modeling is compared to the risk resulting from traditional approaches based on historical data. The streamflow data of the past 50 years (1960-2010) at the location of interest are extracted from the USGS database and used to generate future flood prediction. Two methods have been used for flood prediction with no consideration of climate change; (a) a traditional method where the historic 50-year record is repeated throughout the service life, and (b) a flood prediction based on the Q100-Q500 approach developed by *(19)*. The Q100-

Q500 approach uses the estimated 100-year and 500-year floods (i.e. Q100 and Q500) to randomly generate daily streamflow data. Figures 16a and b shows the time-dependent scour depth and mean risk profiles generated using the 50-year historic data, the Q100-Q500 approach, and the mean of all climate models. It can be seen that there is a considerable difference between the three risk profiles. As shown, the 50-year risk profile tends to underestimate the risk compared to the other two approaches; while the Q100-Q500 predicted, at the end of the service life, approximately double the risk value established using proper climate modeling.

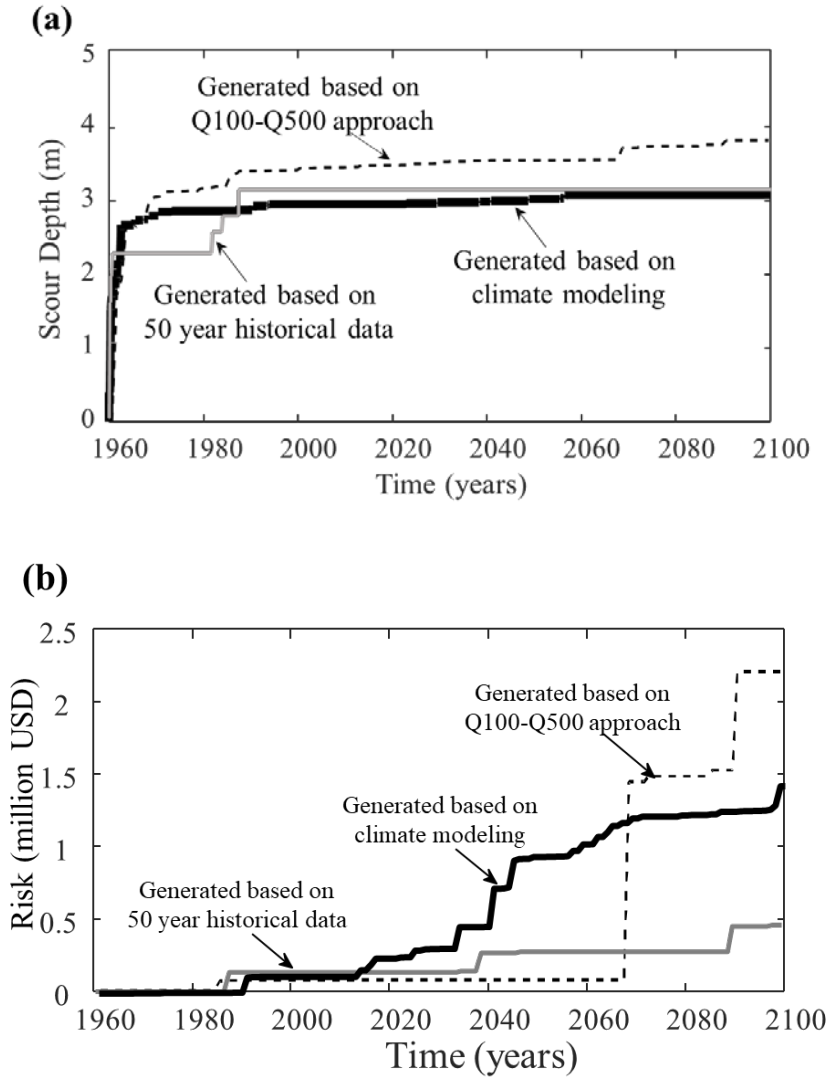

Figure 16. Comparison of time-dependent (a) scour depth (b) risk profile based on climate modeling, 50-year historical data, and Q100-Q500 approach.

5.3. Combined Effects of Flood, Scour, and Marine Corrosion

The previously discussed immersion corrosion approach is applied to the bridge analyzed in this report to quantify the increase of failure risk under corrosion. Since the investigated bridge is not located in a marine environment, this corrosion model may not accurately predict the

corrosion loss for the investigated location. The purpose of this study is to illustrate the application of such model in investigating the potential impacts of climate change.

Historic water and temperature records are adopted from the USGS database. The curve fitting toolbox of MATLAB software *(61)* is next used to draw a relationship between water and air temperature data. The curve fitting results are shown in Figure 17.

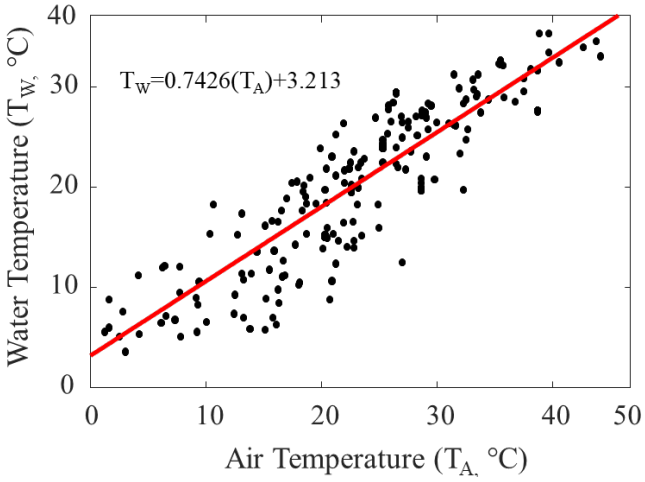

Figure 17. Air and water temperature relationship.

Historical records of dissolved inorganic nitrogen are also adopted from USGS water quality records and their associated probabilistic distribution was obtained using MATLAB distribution fitting tool. The exponential distribution was found to provide the best fit for the DIN historical data. Figure 18 shows the associated histogram and the exponential fit. The adopted temperature profiles corresponding to the nine climate scenarios are next integrated into the presented corrosion prediction approach to generate the time-dependent corrosion loss considering climate change.

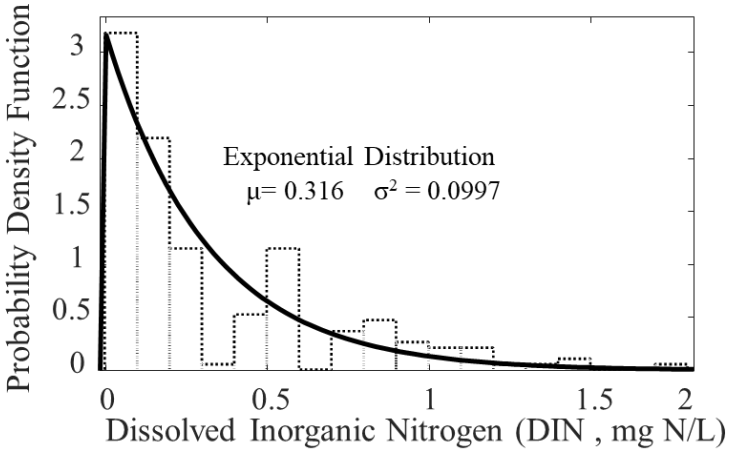

Figure 18. Distribution fitting of DIN records.

In traditional climate projection methods used for structural assessment purposes, future climate behavior is assumed to follow the recorded historic patterns. In order to compare corrosion losses generated from climate modeling to those based on historical temperature

records, the fitted distribution of the recoded water temperature was used to generate the future temperature trends. The fitted distribution of the recorded water temperature data is shown in Figure 19. The recorded water temperature was found to follow a generalized extreme value distribution.

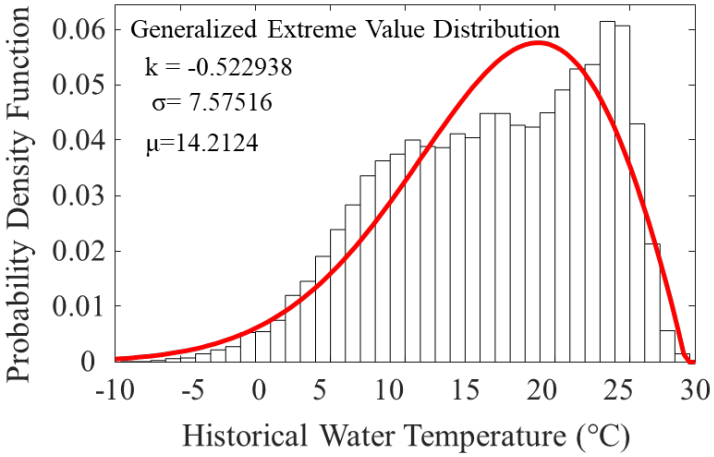

Figure 19. Distribution fitting of water temperature.

The results of the time-dependent corrosion loss predicted based on the climate modeling and the historical records are depicted in Figure 20. It can be seen that the results generated based on the mean of all considered climate scenarios slightly varies from the one generated based on historical data. This difference reaches up to 10% at the year 2100.

The time-dependent risk of failure is finally calculated based on the generated consequences and time-dependent probability of failure. Figure 21 shows the resulting time-dependent risk profiles for the investigated bridge considering the combined effects of flood, flood-induced scour, and marine corrosion.

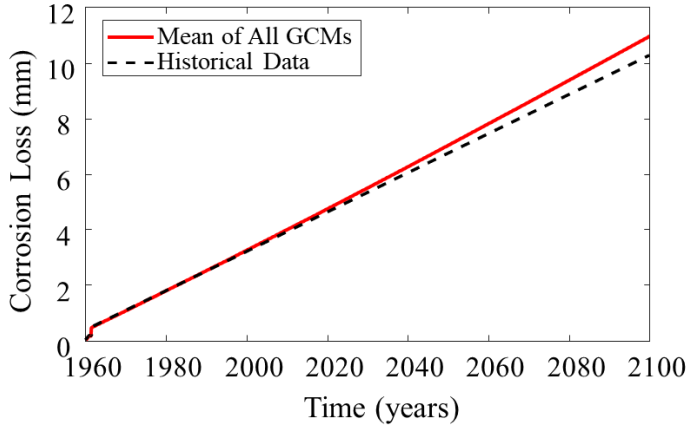

Figure 20. Comparison of time-dependent corrosion loss generated based on GCMs and historical data.

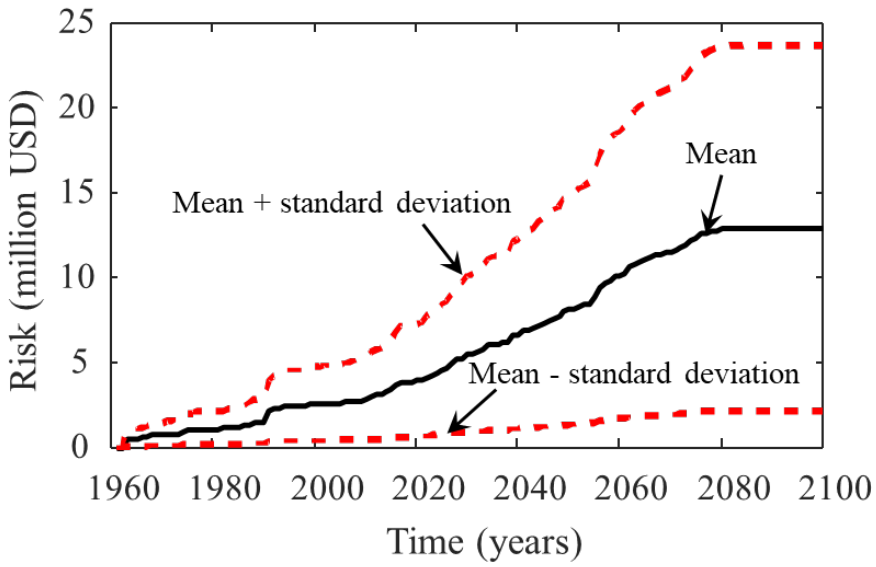

Figure 21. The time-dependent risk considering the combined effects of flood, flood-induced scour, and marine corrosion.

5.4. Combined Effects of Flood, Scour, and Fresh Water Corrosion

As previously discussed, the marine corrosion prediction is not applicable to the cases with fresh water. The Eurocode freshwater corrosion approach is used to establish a time-dependent corrosion loss relationship. This relationship has been produced through a linear fit based on the results of common fresh water in the high zone attack. Figure 22 shows the results of this linear fit.

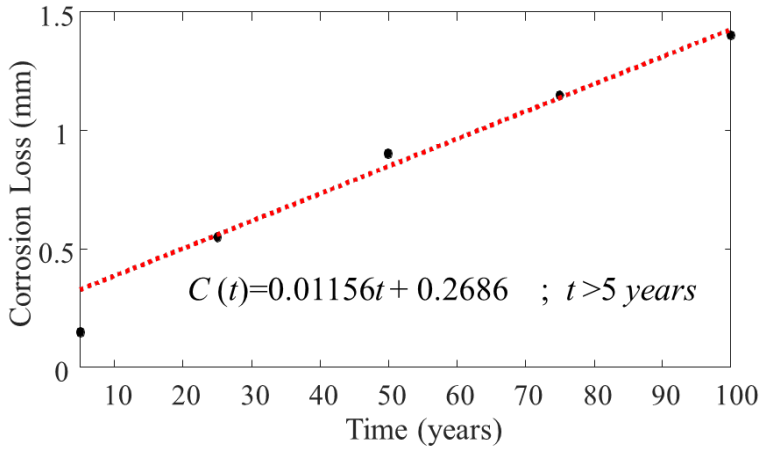

Figure 22. Freshwater time-dependent corrosion loss prediction.

The proposed relationship is then integrated into the analysis of the investigated bridge and the time-dependent risk profile is generated. Figure 23 shows a comparison between the results generated for the case when the bridge is only facing the flood and scour and for the case when it faces the flood, flood-induced scour and freshwater corrosion. It can be seen that in the case considering the freshwater corrosion, the risk is increased dramatically.

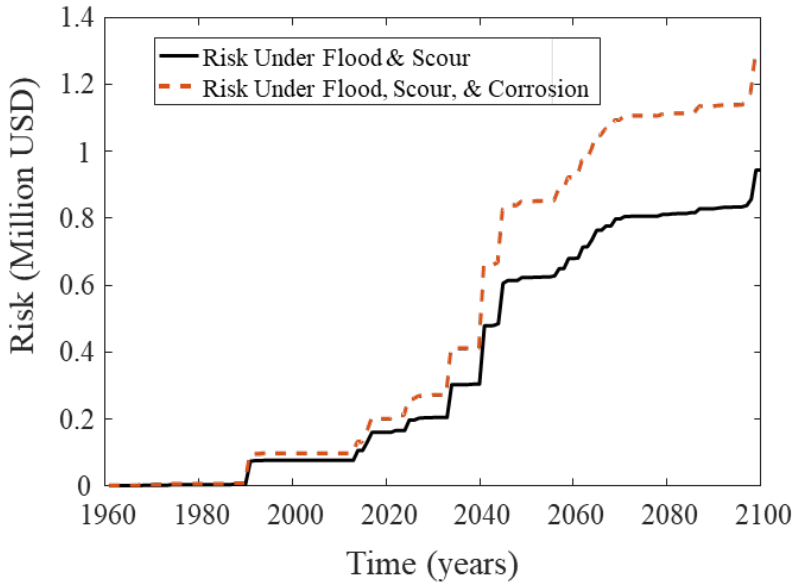

Figure 23. Time-dependent risk profiles considering flood and scour versus flood, scour and freshwater corrosion.

5.5. Optimal Maintenance Planning

After establishing the risk profile, a management plan should be developed with the goal of minimizing the risk or failure probability of the bridge. Other management objectives can also be considered including minimizing the life-cycle cost and extending the service life, among others. Single or multi-objective optimization can be used to establish these management plans. In this case study, a single-objective optimization procedure is presented with the goal of determining the optimal maintenance time of the bridge foundations. The maintenance action is defined herein as the replacement of the bridge foundation. Accordingly, the performance of the bridge foundation is restored to initial condition after the maintenance. The optimization process established the optimal time of foundation replacement that minimizes the maximum life-cycle cumulative probability of failure. The replacement is performed only one time during the service life of the bridge. The optimization problem is formulated as:

Given: $TDP(y)$, t_{sl} [25]

Find: t_{main} [26]

To minimize: maximum life-cycle cumulative probability of failure (TDP_{max}) [27]

where $TDP(y)$, $t_{sl,}$ and t_{main} are cumulative annual probability of failure, service life, and time of maintenance action, respectively. Genetic algorithms employed through the Global Optimization Toolbox of MATLAB *(61)* have been used to solve this optimization problem. Integer genetic algorithm has been implemented; accordingly, the solver attempts to minimize a penalty function rather than the fitness function. The penalty function, which includes a term for infeasibility, is combined with binary tournament selection to select individuals for subsequent generations *(61)*. Figure 24 shows the mean and best penalty values for each generation. The optimum time for foundation replacement is at the year 2032. Figure 25 compares the annual probability of failure for the optimal maintenance plan to non-optimal

plans performed at different times along the service life. As shown, the optimum maintenance plan succeeds in predicting the lowest maximum annual probability of failure value.

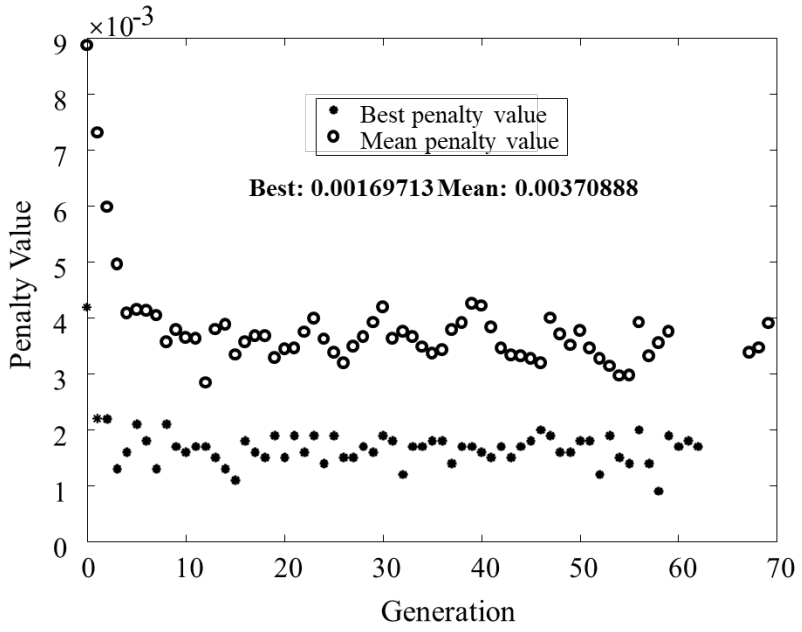

Figure 24. Mean and best penalty values versus generations.

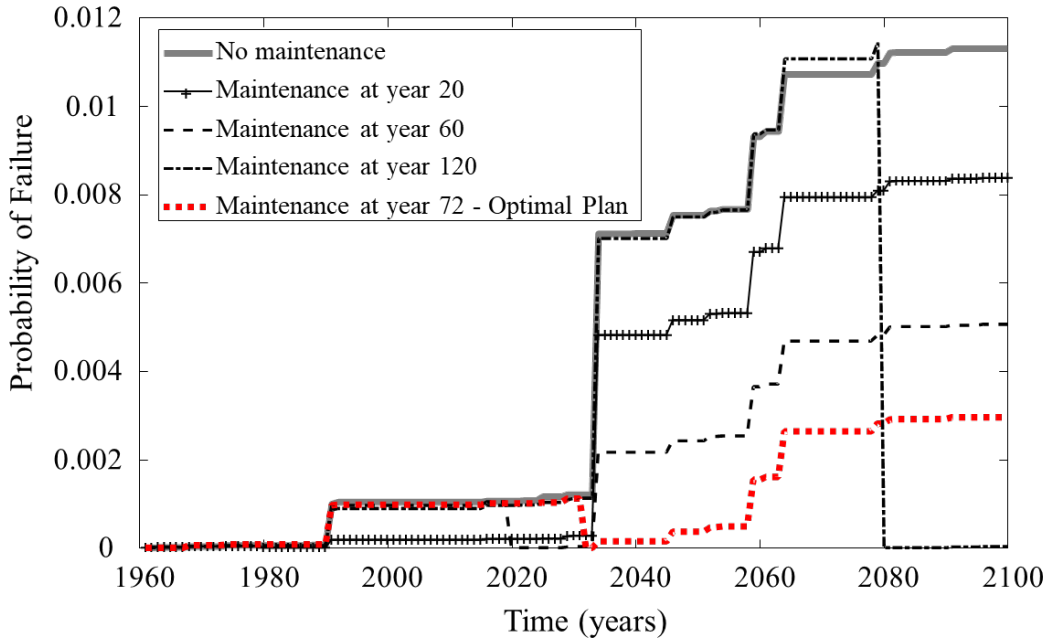

Figure 25. Comparison of annual cumulative probability of failure based on different maintenance plans.

In a similar manner, more maintenance options can be integrated into the optimization process, including those associated with other bridge components such as the girders and deck *(69)*. In addition, multi-objective optimization can be defined to simultaneously minimize the failure probability while minimizing the life-cycle cost *(70, 71)*.

6. CONCLUSIONS

This research project presented a risk-based probabilistic framework for optimizing the management activities of bridges susceptible to damage due to sudden hazards and gradual deteriorative effects. The framework predicts the risk of failure considering the effects of climate change using downscaled data of global climate models. The downscaled precipitation and temperature Climate data are adopted from CMIP5 archive for the location of interest during the time span of 1960 to 2100. The IHACRES statistical model is used to convert the climate data to streamflow hydrographs at the bridge location. Time-dependent scour depth is quantified and its effect on the axial and lateral capacity of the bridge foundation is computed. The annual point-in-time failure probability of the bridge due to flood-induced loads is used to predict the cumulative failure probability profiles of the bridge. After evaluating the consequences associated with bridge failure, the time variant bridge risk profile is established. In addition, a risk-based probabilistic framework for optimizing the management activities of bridges susceptible to damage due to floods, flood-induced scour, and corrosive environment is presented in this report. Two cases of marine corrosion and freshwater corrosions are examined in this study. The following conclusions are drawn:

- The results indicate that the time-variant corrosion losses have low sensitivity to the adopted climate scenario. However, scour modeling is highly dependent on the climate model and its parameters. Traditional methods for streamflow and corrosion loss prediction based on historic data underestimate or over-predict the risk of bridge failure depending on the assumptions used to establish the future streamflow data. In contrast, the proposed approach based on climate modeling provides a rational prediction of future risk while properly accounting for the effect of future climate change.
- The analysis of predicted streamflow considering climate data for the location of interest indicates that although the mean annual discharge had a general decreasing trend, the maximum annual discharge (i.e., flow peaks) shows a steady increase. This highlights the importance of proper climate modeling during bridge risk assessment.
- The time-variant scour depth significantly depends on the adopted climate scenarios. A variation of 29% in the final scour depth predicted using the different climate scenarios has been observed at the studied location. Accordingly, a probabilistic approach considering all potential scenarios is necessary to properly quantify the risk of bridge failure due to flood and flood-induced scour hazards.
- The MPI-ESM-LR model predicts the most aggressive time-dependent scour depth profile while MIROC5 model predicts the smallest scour depth profiles. In addition, the RCP 2.6 associated with each model predicts the biggest scour depth, while the 8.5 RCP values predict the smallest scour depth profiles.

7. RECOMMENDATIONS

- The proposed optimization framework can establish the optimum maintenance solutions which can minimize the failure probability of the bridge under investigation. The use of such detailed analysis approaches is recommended over traditional bridge management tools relying on simplified assumptions on bridge condition states.
- Traditional methods for streamflow prediction based on historic data can underestimate or over-predict the risk of bridge failure under flood and flood-induced scour depending on the assumptions used to establish the future streamflow data. In contrast, the proposed probabilistic approach based on climate models provides a rational prediction of future risk while properly accounting for uncertainties associated with future climate and flood conditions. It is recommended to perform such analysis for new bridge construction or for establishing management plans for existing bridges.
- Selection of appropriate climate scenarios should be based on a detailed comparison of their past predictions with the historical records.
- The framework presented in this study can be easily applied to other bridge cases. This can be achieved by adjusting the foundation parameters, failure modes, and updating the location for the climate modeling module.

REFERENCES

1. Knittle, A., Naifeh, L., (2015). Flooding continues to hamper parts of Oklahoma. Retrieved from: https://newsok.com/article/5429371/flooding-continues-to-hamper-parts-of-oklahoma

2. AASHTO. (2010). American association of state highway and transportation officials (LRFD) bridge design specifications. 5th Ed., Washington, DC.

3. Briaud, J. L., Gardoni, P., & Yao, C. (2013). Statistical, risk, and reliability analyses of bridge scour. Journal of Geotechnical and Geoenvironmental Engineering, 140(2), 04013011.

4. Cook, W., Barr, P.J., & Halling, M.W. (2015). Bridge failure rate. Journal of Performance of Constructed Facilities, 29(3), 04014080.

5. NOAA (2017). National Oceanic and Atmospheric Administration, http://www.noaa.gov/

6. Fechter, J. (2015). TXDoT: Two bridges completely wrecked in Central Texas floods, others damaged. Retrieved from: http://www.mysanantonio.com/news/local/article/TXDoT-Two-bridges-wrecked-in-the-Central-Texas-6294892.php#photo-8045574

7. Danner, C., & Fuller, J., (2015). Texas and Oklahoma begin cleaning up after devastating floods. Retrieved from: http://nymag.com/daily/intelligencer/2015/05/floods-devastate-texas-and-oklahoma.html

8. Smith, A., Lott, N., Houston, T., Shein, K., Crouch, J., & Enloe, J. (2017). US billion-dollar weather & climate disasters: 1980-2017. NOAA National Centers for Environmental Information. https://www.ncdc.noaa.gov/billions/events.pdf.

9. Ettouney, M. M., & Alampalli, S. (2011). Infrastructure Health in Civil Engineering: Applications and Management. CRC Press, Taylor and Francis Boca Raton, Florida.

10. Hung, C.-C., & Yau, W.-G. (2014). Behavior of scoured bridge piers subjected to flood-induced loads. Engineering Structures, 80, 241-250.

11. Banerjee, S., & Ganesh Prasad, G. (2013). Seismic risk assessment of reinforced concrete bridges in flood-prone regions. Structure and Infrastructure Engineering, 9(9), 952-968.

12. Ganesh Prasad, G., & Banerjee, S. (2013). The impact of flood-induced scour on seismic fragility characteristics of bridges. Journal of Earthquake Engineering, 17(6), 803-828.

13. Stewart MG, Wang X, Nguyen MN. Climate change impact and risks of concrete infrastructure deterioration. Engineering Structures. 2011; 33(4):1326-37.

14. Stewart MG, Wang X, Nguyen MN. Climate change adaptation for corrosion control of concrete infrastructure. Structural Safety. 2012; 35:29-39.

15. Chaves IA, Melchers RE, Peng L, Stewart MG. Probabilistic remaining life estimation for deteriorating steel marine infrastructure under global warming and nutrient pollution. Ocean Engineering. 2016; 126:129-37.

16. Peng L, Stewart MG, Melchers RE. Corrosion and capacity prediction of marine steel infrastructure under a changing environment. Structure and Infrastructure Engineering. 2017; 13(8):988-1001.

17. Govindasamy, A.V., Briaud, J., Chen, H., Delphia, J., Elsbury, K., Gardoni, P., Herrman, G., Kim, D., Mathewson, C., McClelland, M., & Olivera, F. (2008). Simplified method for estimating scour at bridges,GeoCongress 2008, Geosustainability and Geohazard Mitigation, 178, 385-393.

18. Arneson, L.A., Zevenbergen, L.W., Lagasse, P.F., & Clopper, P.E. (2012). Evaluating scour at bridges. Hydraulic Engineering Circular No. 18: FHWA-HIF-12-003, U.S. DOT, Washington, DC.

19. Briaud, J.-L., Brandimarte, L., Wang, J., & D'Odorico, P. (2007). Probability of scour depth exceedance owing to hydrologic uncertainty. Georisk: Assessment and Management of Risk for Engineered Systems and Geohazards, 1(2), 77-88.

20. Bolduc, L., Gardoni, P., & Briaud, J.-L. (2008). Probability of exceedance estimates for scour depth around bridge piers, Journal of Geotechnical and Geoenvironmental Engineering, 134(2), 175–184.

21. Decò, A., & Frangopol, D. M. (2011). Risk assessment of highway bridges under multiple hazards. Journal of Risk Research, 14(9), 1057-1089.

22. Wang, Z., Padgett, J.E., & Dueñas-Osorio, L. (2014). Risk-consistent calibration of load factors for the design of reinforced concrete bridges under the combined effects of earthquake and scour hazards. Engineering Structures, 79, 86-95.

23. Alipour, A., & Shafei, B. (2012). Performance assessment of highway bridges under earthquake and scour effects. In Proceedings of the 15th world conference on earthquake engineering, Lisbon, Portugal. 24-28.

24. Yilmaz, T., Banerjee, S., & Johnson, P.A. (2016). Performance of two real-life California bridges under regional natural hazards. Journal of Bridge Engineering, 21(3), 04015063.

25. Gehl, P., & D'Ayala, D. (2016). Development of Bayesian networks for the multi-hazard fragility assessment of bridge systems. Structural Safety, 60, 37-46.

26. Zhu, B., & Frangopol, D. M. (2016a). Time-dependent risk assessment of bridges based on cumulative-time failure probability. Journal of Bridge Engineering, 21(12), 06016009.

27. Zhu, B., & Frangopol, D. M. (2016b). Time-variant risk assessment of bridges with partially and fully closed lanes due to traffic loading and scour. Journal of Bridge Engineering, 21(6), 04016021.

28. Kallias, A. N., & Imam, B. (2016). Probabilistic assessment of local scour in bridge piers under changing environmental conditions. Structure and Infrastructure Engineering, 12(9), 1228-1241.

29. Dong, Y., & Frangopol, D. M. (2016). Probabilistic time-dependent multihazard life-cycle assessment and resilience of bridges considering climate change. Journal of Performance of Constructed Facilities, 30(5), 04016034.

30. Anderson, C. J., Claman, D., & Mantilla, R. (2015). Iowa's Bridge and Highway Climate Change and Extreme Weather Vulnerability Assessment Pilot.

31. Sheffield, J., Barrett, A. P., Colle, B., Nelun Fernando, D., Fu, R., Geil, K. L., Hu, Q., Kinter, J., Kumar, S. & Langenbrunner, B. (2013a). North American climate in CMIP5 experiments. Part I: evaluation of historical simulations of continental and regional climatology. Journal of Climate, 26(23), 9209-9245.

32. Sheffield, J., Camargo, S. J., Fu, R., Hu, Q., Jiang, X., Johnson, N., Karnauskas, K. B., Kim, S. T., Kinter, J. & Kumar, S. (2013b). North American climate in CMIP5 experiments. Part II: evaluation of historical simulations of intraseasonal to decadal variability. Journal of Climate, 26(23), 9247-9290.

33. Taylor, K. E., Stouffer, R. J., & Meehl, G. A. (2012). An overview of CMIP5 and the experiment design. Bulletin of the American Meteorological Society, 93(4), 485-498.

34. Laprise, R. (2008). Regional climate modelling. Journal of Computational Physics, 227(7), 3641-3666.

35. Coiffier, J. (2011). Fundamentals of numerical weather prediction. Cambridge University Press.

36. Xue, Y., Janjic, Z., Dudhia, J., Vasic, R., & De Sales, F. (2014). A review on regional dynamical downscaling in intraseasonal to seasonal simulation/prediction and major factors that affect downscaling ability. Atmospheric research, 147, 68-85.

37. Liang, X., Lettenmaier, D. P., Wood, E. F., & Burges, S. J. (1994). A simple hydrologically based model of land surface water and energy fluxes for general circulation models. Journal of Geophysical Research: Atmospheres, 99(D7), 14415-14428.

38. David, C. H., Famiglietti, J. S., Yang, Z. L., Habets, F., & Maidment, D. R. (2016). A decade of RAPID—Reflections on the development of an open source geoscience code. Earth and Space Science, 3(5), 226-244.

39. Zagona, E. A., Fulp, T. J., Shane, R., Magee, T., & Goranflo, H. M. (2001). RiverWare: A generalized tool for complex reservoir system modeling. JAWRA Journal of the American Water Resources Association, 37(4), 913-929.

40. McPherson, R., (2016). SCCSC, South Centeral Climate Science Center. Impacts of Climate change on Flows in the Red River Basin, Final Report, Feb. 2016.

41. Solomon, S. (Ed.). (2007). Climate change 2007-the physical science basis: Working group I contribution to the fourth assessment report of the IPCC (Vol. 4). Cambridge University Press.

42. Stocker, T., Qin, D., Plattner, G., Tignor, M., Allen, S., Boschung, J., Nauels, A., Xia, Y., Bex, B. & Midgley, B. (2013). IPCC, The physical science basis. Contribution of working group I to the fifth assessment report of the intergovernmental panel on climate change.

43. Maloney, E. D., Camargo, S. J., Chang, E., Colle, B., Fu, R., Geil, K. L., Hu, Q., Jiang, X., Johnson, N. & Karnauskas, K. B. (2014). North American climate in cmip5 experiments: part iii: assessment of twenty-first-century projections. Journal of Climate, 27(6), 2230-2270.

44. Hidalgo, H. G., & Alfaro, E. J. (2015). Skill of CMIP5 climate models in reproducing 20th century basic climate features in Central America. International Journal of Climatology, 35(12), 3397-3421.

45. Maurer, E. P., & Hidalgo, H. G. (2008). Utility of daily vs. monthly large-scale climate data: an intercomparison of two statistical downscaling methods. Hydrology and Earth System Science, 12, 551-563.

46. Maurer, E. P., Hidalgo, H. G., Das, T., Dettinger, M. D., & Cayan, D. R. (2010). The utility of daily large-scale climate data in the assessment of climate change impacts on daily streamflow in California. Hydrology and Earth System Science, 14, 1125-1138.

47. Shrestha, B., Cochrane, T. A., Caruso, B. S., Arias, M. E., & Piman, T. (2016). Uncertainty in flow and sediment projections due to future climate scenarios for the 3S Rivers in the Mekong Basin. Journal of Hydrology, 540, 1088-1104.

48. Brekke, L., Thrasher, B. L., Maurer, E. P., & Pruitt, T. (2013). Downscaled CMIP3 and CMIP5 climate and hydrology projections: Release of downscaled CMIP5 climate projections, comparison with preceding information, and summary of user needs. US Department of the Interior, Bureau of Reclamation, Technical Services Center, Denver, Colorado, USA.

49. Croke, B. F. W., & Jakeman, A. J. (2008). Use of the IHACRES rainfall-runoff model in arid and semi arid regions. Hydrological modelling in arid and semi-arid areas, 41-48.

50. Carcano, E. C., Bartolini, P., Muselli, M., & Piroddi, L. (2008). Jordan recurrent neural network versus IHACRES in modelling daily streamflows. Journal of hydrology, 362(3), 291-307.

51. Croke, B. F. W., Andrews, F., Spate, J., & Cuddy, S. M. (2005). IHACRES user guide. Technical Report 2005/19. Second Edition. iCAM, School of Resources, Environment and Society, The Australian National University, Canberra.

52. Ye, W., Bates, B. C., Viney, N. R., Sivapalan, M., & Jakeman, A. J. (1997). Performance of conceptual rainfall-runoff models in low-yielding ephemeral catchments. Water Resources Research, 33(1), 153-166.

53. Gudavalli, R., Ting, F. C. K., Briaud, J. L., Chen, H. C., Perugu, S., & Wei, G. (1997). Flume tests to study scour rate of cohesive sails. Res. Rep. Prepared for Texas Dept. of Transp.

54. USGS (2017). United State Geological Survey, National Water Information Service, https://waterdata.usgs.gov/nwis

55. Briaud, J. L., Ting, F. C., Chen, H. C., Gudavalli, R., Perugu, S., & Wei, G. (1999). SRICOS: Prediction of scour rate in cohesive soils at bridge piers. Journal of Geotechnical and Geoenvironmental Engineering, 125(4), 237-246.

56. Prasad, Y. V., & Chari, T. R. (1999). Lateral capacity of model rigid piles in cohesionless soils. Soils and Foundations, 39(2), 21-29.

57. Hannigan, P. J., Goble, G. G., Thendean, G., Likins, G. E., & Rausche, F. (1997). Design and construction of driven pile foundations-Volume ii (No. FHWA-HI-97-014).

58. Reese, L. C., & Van Impe, W. F. (2010). Single piles and pile groups under lateral loading. CRC Press.

59. AASHTO. (2014). American association of state highway and transportation officials (LRFD) bridge design specifications. 6th Ed., Washington, DC.

60. Cuomo, G., Shams, G., Jonkman, S., & Van Gelder, P. (2008). Hydrodynamic loadings of buildings in floods. Coastal Engineering, 3745.

61. MathWorks, M. A. T. L. A. B. (2016). SIMULINK for technical computing. Available on http://www. rnathworks. com.

62. Stein, S. M., Young, G. K., Trent, R. E., & Pearson, D. R. (1999). Prioritizing scour vulnerable bridges using risk. Journal of Infrastructure Systems, 5(3), 95-101.

63. Melchers RE. Modeling of Marine Immersion Corrosion for Mild and Low-Alloy Steels—Part 2: Uncertainty Estimation. Corrosion. 2003; 59(4):335-44.

64. Melchers RE. Long-term immersion corrosion of steels in seawaters with elevated nutrient concentration. Corrosion Science. 2014; 81:110-6.

65. USGS (2017). United State Geological Survey, Earthquake Hazard Program, https://earthquake.usgs.gov/hazards/

66. Ellsworth, W. L. (2013). Injection-induced earthquakes. Science, 341(6142), 1225942.

67. FHWA (Federal Highway Administration). (2016). National bridge inventory (NBI) dataset. Retrieved from: https://www.fhwa.dot.gov/bridge/nbi/ascii2016.cfm

68. Fellenius B.H. (1991) Pile Foundations. In: Fang BY. (eds) Foundation Engineering Handbook. Springer, Boston, MA.

69. Okasha, N. M., & Frangopol, D. M. (2010). Novel approach for multicriteria optimization of life-cycle preventive and essential maintenance of deteriorating structures. Journal of Structural Engineering, 136(8), 1009-1022.

70. Barone, G., Frangopol, D. M., & Soliman, M. (2013). Optimization of life-cycle maintenance of deteriorating bridges with respect to expected annual system failure rate and expected cumulative cost. Journal of Structural Engineering, 140(2), 04013043.

71. Soliman, M., Frangopol, D. M., & Kim, S. (2013). Probabilistic optimum inspection planning of steel bridges with multiple fatigue sensitive details. Engineering Structures, 49, 996-1006.